Arch. Mech., 49, 5, pp. 919–962, Warszawa 1997

Large scale motion and temperature distributions in land-based ice shields; the Greenland Ice Sheet in response to various climatic scenarios

R. CALOV and K. HUTTER (DARMSTADT)

Dedicated to Prof. Franz Ziegler on the occasion of his 60-th birthday

A REVIEW IS GIVEN of the theory of cold ice sheets in the so-called shallow ice approximation, and a literature survey is performed of its application in ice sheet modelling of the large ice shields, such as Greenland, Antarctica and other, historical, ice sheets. As model applications, steady state and time-dependent computations are performed for the Greenland Ice Sheet using an ice sheet model on the basis of the 3-D shallow ice equations of a viscous, heat-conducting incompressible fluid. The interaction with the solid earth is through a heat-conducting homogeneous isotropic rigid solid subjected to geothermal heat. The climate driving is effected through a prescribed atmospheric surface temperature and accumulation rate function. Computations are performed for the ice-thickness distribution to steady driving conditions when external and internal parameters are varied. It is shown that the sliding coefficient and the amplitude of the annual temperature variation are particularly critical. Finally, the evolution of the basal temperature distribution at Dye 3, Summit and Camp Century through idealized scenarios of the ice age(s) is computed; these computations show that the basal temperature regime depends critically on the thermal inertia of the bedrock and the magnitude of the ice fluidity. Our computations with various climate state scenarios demonstrate how well the model reproduces the measured flow data in Greenland and indicates how it must be extended to accomodate the polythermal structure of the ice and to include longitudinal stretching effects.

1. Introduction

FIRST AD-HOC DESCRIPTIONS of the distributions of velocity, temperature and evolution of the geometry of ice sheets are largely due to NYE [138-151, 153], GLEN [48, 65], LLIBOUTRY [107–116], WEERTMAN [178–187] and others; however, while these works contain the essential ingredients of the theoretical formulation and systematic development of a mathematical boundary value problem, rational deduction of the latter had to await the works of FOWLER [37–40, 41–46], HUTTER [66–72, 78, 79, 61–63] and MORLAND [131–137].

Computational results are presented here on the flow, temperature and geometry of the Greenland Ice Sheet in response to various climate scenarios using an ice sheet model that is based on the Shallow Ice Approximation [25, 26]. The growth and retreat of inland ice masses is governed by the snowfall onto the surface, the melting and calving of the ice close to and at the outer ice boundaries. Owing to its own weight, the ice deforms with velocities of typically $100\,\mathrm{m\,a^{-1}}$ causing a transport of ice towards the ice sheet boundaries where the ice melts and calves. This process, in turn, is influenced by the temperature distribution within the ice, implying a delicate balance between the thermal and mechanical regimes that are established by the climate input and the geothermal conditions of the substrate. The thermomechanically coupled ice dynamics together with the mass flux due to snowfall and mass loss in the vicinity of ice boundaries determine the thickness distribution of a particular ice sheet.

The deformation of an ice sheet and the variation of its temperature distribution depends to a large extent on its thermomechanical constitutive modelling. Here, we treat ice as a rheologically nonlinear, thermally coupled, viscous fluid, i.e., we assume its fluidity (inverse viscosity) to be temperature-dependent, the latter according to a power law with exponent $n = 3$, the former essentially following an Arrhenius-type relationship. When the temperature reaches the melting point, it is held at pressure melting without accounting energetically for the water production. This body is subject to driving mechanisms from the outside world that are imposed on the ice sheet via its surrounding boundaries. At its bottom we account for the presence of a heat-conducting rigid solid of 4 km thickness. At the free surface, the climate input is effected by the prescription of the mean annual atmospheric temperature and accumulation rate fuctions; the latter expresses the rate of mass added and subtracted according to the amount of snowfall and melting of surface ice, respectively. At the base, a relatively complex viscous-type sliding law is implemented and a thermodynamic jump condition of heat flow provides the connection with the heat-conducting lithosphere. As for the former, the no-slip condition applies where the basal ice is below the pressure melting point, but a power law relationship between shear traction and sliding velocity is imposed when the basal ice is at the pressure melting point. At the lower boundary of the rigid substrate the geothermal heat flow is prescribed.

By using standard climate driving functions (constant climate and idealized interglacial variations) for the surface temperature and mass balance, we study the reaction of the Greenland Ice Sheet to (i) variations in the parameterization of the driving functions, (ii) the viscous-type basal sliding law, (iii) the apparent viscosity (fluidity) of the ice and (iv) the role played by the thermal inertia of the rock bed. In particular it is shown that the amplitude of the annual variation of the surface temperature and the drag coefficient of the basal sliding law are critical for climate stability of large ice sheets.

Furthermore, using several reasonable climate scenarios for the past, and numerical values for the material and climate parameters appropriate for Green-

land, it is shown that, while the temperate patches at the base always existed, the locations of Dye 3, Camp Century and Summit were always cold.

2. The model

A review is presented of the governing equations of ice sheet dynamics: how they emerge from first principles of continuum thermodynamics, how the equations have been simplified by an asymptotic analysis that is based on a shallowness assumption, and what mathematical-numerical difficulties arise in using this shallow ice approximation (SIA). The intention is to present to the reader an up-to-date state-of-the-art which is fairly complete; as far as the current literature goes, we cannot claim, however, that the cited literature is exhaustive.

2.1. Field equations

The ice in large ice masses (Fig. 1) is generally polythermal, i.e., the ice mass consists of disjoint regions in which the ice is either cold (i.e., its temperature is below the melting point) or temperate (i.e., it is at the pressure melting point), but except for a few very recent cases [5, 7, 45, 68, 74, 75, 76, 47, 49–56], theoretical formulations are restricted to *cold ice*. For such a case the continuum mechanical postulate "ice is an incompressible heat-conducting nonlinear viscous

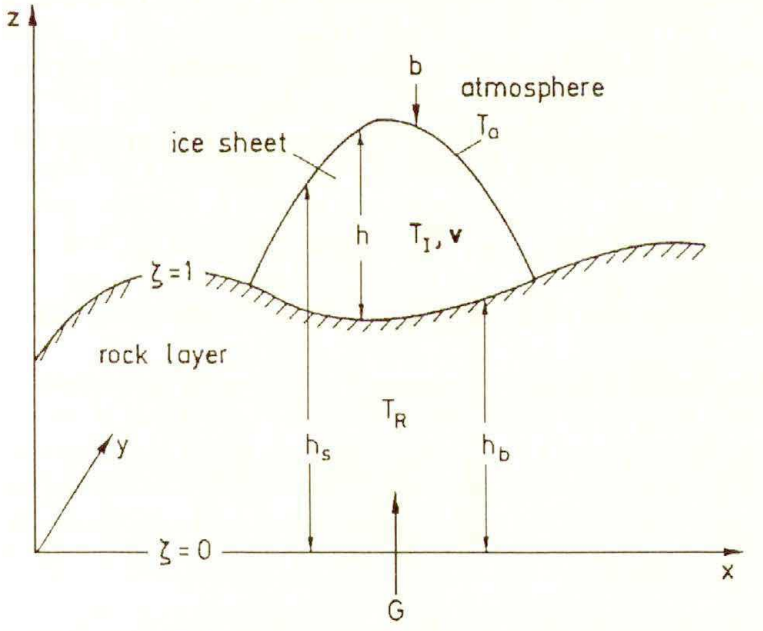

FIG. 1. Model variables with the coordinate system for the ice sheet and the lithosphere layer.

fluid" yields the following balance laws of mass, momentum and energy as well as constitutive relations:

$$
\begin{aligned}
\operatorname{div}\mathbf{v} &= 0,\\
\varrho\dot{\mathbf{v}} &= -\operatorname{grad} p + \operatorname{div}\boldsymbol{\sigma} + \varrho\mathbf{g},\\
\varrho\dot{\varepsilon} &= -\operatorname{div}\mathbf{q} + \operatorname{tr}(\boldsymbol{\sigma}'\mathbf{D}),\\
\varepsilon &= \int_0^T C_p(\bar{T})d\bar{T} + \varepsilon_0,\\
\mathbf{q} &= -\chi(T)\operatorname{grad} T,\\
\mathbf{D} &= \operatorname{sym}(\operatorname{grad}\mathbf{v}) = EA(T')f(I\!I_{\sigma'})\boldsymbol{\sigma}',
\end{aligned}
\tag{2.1}
$$

in which $\mathbf{v}$, ϱ, p, σ', $\mathbf{g}$, ε, $\mathbf{q}$, c_p, χ_I are, respectively, the velocity vector, ice density, pressure, Cauchy stress deviator (i.e., $\operatorname{tr}(\sigma') = 0$, where $\operatorname{tr}(\cdot)$ is the trace operator), specific gravity, internal energy, heat flux vector, specific heat (at constant pressure) and heat conductivity. Furthermore,

$$
T' = T + ap, \qquad A(T') = A_0 \exp\left(-\frac{Q}{R(T_0+T')}\right), \qquad I\!I_\sigma = \frac{1}{2}\operatorname{tr}(\boldsymbol{\sigma}'^2),
\tag{2.2}
$$

where T' is the homologous temperature, a the Clausius–Clapeyron constant, A a temperature-dependent rate factor, $f(I\!I_{\sigma'})$ the fluidity with $n = 3$ and E a so-called enhancement factor. The power law fluidity has been introduced into glaciology by NYE [141] and GLEN [48] but should be replaced by a finite viscosity law because of its singular behaviour at small stretchings (HUTTER [71] and MORLAND [134]) when $n > 1$. For its experimental justification, see [8, 24, 29, 33, 34, 106, 168]. The enhancement factor E accounts for the apparent different flow properties of Holocene and Pleistocene ice [28, 29, 31]. Up to today $E = E(\mathfrak{A})$ is assumed to be a function of age with values $E = 1$, for Holocene, and $E = 3$, for Pleistocene ice, and $\mathfrak{A}$ satisfies the differential equation([1]) $\dot{\mathfrak{A}} = 1$. A_0 is a constant, Q the activation energy of ice, R the gas constant and $T_0 = 273.15\,\mathrm{K}$ the melting temperature at normal pressure (10^5 Pa). Numerical values are given in Table 1.

The above model (2.1), (2.2) is standard except for the occurrence of E. From a thermodynamic point of view, this variable has the meaning of an internal variable and was first introduced into a theoretical model by HUTTER and VULLIET [77]. Glaciologists are generally unaware of this and use it as a fudge factor. More important than this is the fact that the above fluid model is necessarily isotropic and thus cannot describe stress-induced anisotropies evident in specimens from boreholes [27, 49, 117, 130, 174, 175].

([1]) An initial distribution of $\mathfrak{A}$ and the values of $\mathfrak{A}$ of any ice particle at the time when it is formed must be prescribed. Since ice is accumulated at the free surface, this essentially amounts to prescribing $\mathfrak{A}(t_0)$, $t_0 < t$ on those parts of the free surface where snow is accumulating.

Table 1. Physical constants used in ice sheet models.

Earth's acceleration g		$9.81\ \mathrm{m\,s^{-2}}$
Density	Ice ϱ	$0.9\cdot 10^{3}\ \mathrm{kg\,m^{-1}}$
Heat conduction	Ice χ	$2.1\ \mathrm{W\,m^{-1}K^{-1}}$
	Rock χ_R	$3\ \ \mathrm{W\,m^{-1}K^{-1}}$
Thermal diffusivity	Ice κ	$1.15\cdot 10^{-6}\ \mathrm{m^2s^{-1}}$
	Rock κ_R	$1.5\cdot 10^{-6}\ \mathrm{m^2s^{-1}}$
Specific heat of ice C_v		$2009\ \mathrm{J\,kg^{-1}K^{-1}}$
Clausius–Clapeyron constant a		$7.42\cdot 10^{-5}\ \mathrm{K(kPa)^{-1}}$
Latent heat of fusion for ice L_s		$335\cdot 10^{3}\ \mathrm{J\,kg^{-1}}$
Geothermal heat flow G		$42\cdot 10^{-3}\ \mathrm{Wm^{-2}}$
Power law exponent n		3
Gas constant R		$8.314\ \mathrm{J\,mol^{-1}\,K^{-1}}$
Rate factor A_0	$T' \geq -10°\mathrm{C}$	$6.3\times 10^{10}\ \mathrm{a^{-1}\,Pa^{-3}}$
	$T' < -10°\mathrm{C}$	$1.3\times 10^{-5}\ \mathrm{a^{-1}\,Pa^{-3}}$
Activation energy Q	$T' \geq -10°\mathrm{C}$	$139\ \mathrm{kJ\,mol^{-1}}$
	$T' < -10°\mathrm{C}$	$60\ \mathrm{kJ\,mol^{-1}}$

This thermomechanical model for the ice is coupled to the heat conduction equation of a rigid substratum

$$\varrho c_R \dot{T}_R = \mathrm{div}(\chi_R \mathrm{grad} T_R) = \chi_R \triangle T_R \tag{2.3}$$

(R for rock), the evolution equations for the ice thickness $h = h_s - h_b$,

$$\frac{\partial h}{\partial t} + \nabla_H \cdot \mathbf{V}_H = b_s + b_b\,, \qquad \mathbf{V}_H = \int_{h_b}^{h_s} \mathbf{v}_H\, dz \tag{2.4}$$

as well as bed sinking

$$\frac{\partial h_b}{\partial t} = -\frac{1}{\tau_l}\left(h_b - h_0 + \frac{\varrho}{\varrho_a} h\right). \tag{2.5}$$

In (2.3) T_R and χ_R are the temperature and heat conductivity of the rock; radio-active heating of the rock is ignored, so as are the contributions due to internal stresses and dissipation. In this sense, the substratum is rigid; however, motions due to bedrock sinking are incorporated in the convective terms (contained in $\dot{T}_R$) and described by (2.5). In Eq. (2.4) $\mathbf{v}_H$ and $\mathbf{V}_H$ are the horizontal velocity components of the ice and its horizontally integrated flux, respectively, and $\nabla_H = (\partial x, \partial y)$. Furthermore, b_s and b_b are the accumulation/ablation and basal melting rate functions, respectively; since basal melting is small, b_b is often

ignored. Formally, (2.4) is a vertically integrated mass balance. Finally, (2.5) is a relaxation-type relationship for the vertical position of the basal boundary of the ice; it models the bed adjustment with the relaxation time $\tau_l \approx 3 \div 5 \times 10^3$ a; h_0 is the relaxed, undisturbed bed topography and ϱ_a the density of the asthenosphere.

Other models of bedrock sinking have also been used, e.g. a diffusion equation

$$\frac{\partial h_b}{\partial t} = D_a \triangle_H (h_b - h_0 + w_a), \tag{2.6}$$

where $D_a = 0.5 \times 10^8$ m^{2}a^{-1} is the asthenosphere diffusivity, $\triangle_H$ the two-dimensional Laplacian and w_a the deflection of the constant thickness lithosphere for which the plate equation

$$D \triangle \triangle w_a = q - \varrho_m w_a,$$
$$q = \begin{cases} \varrho g h, & \text{if} \quad \dfrac{\varrho}{\varrho_R} + h_{sl} \leq h, \\ \varrho_R g (h_{sl} - h), & \text{if} \quad -\dfrac{\varrho}{\varrho_R} + h_{sl} > h \end{cases} \tag{2.7}$$

is solved, where D is the bending rigidity of the lithosphere (10^{25} N m), ϱ_R the density of the mantle (3300 kg m^{-3}) and $h_{sl} =$ is a constant, see [82, 176]. Models which treat the lithosphere as thermoviscoelastic and the asthenosphere as nonlinearly viscous have also been proposed, TURCOTTE and SCHUBERT [176], but so far not implemented in ice sheet models.

If in the solution of the above equations the ice temperature at any point should reach values above the melting point, it is set back to $T = T_M$, and the energy equation is disregarded in these points. Regions where $T = T_M$ are defined as temperate. Thus the thermal processes are not accounted for in these regions, by e.g. calculating the production of water via dissipation and latent heat of fusion, what makes the model approximate.

2.2. Boundary conditions

Boundary conditions that close the equations to a complete boundary value problem must be formulated at the free surface, the ice-bedrock interface, the lower boundary of the rock bed and the ice margins.

At the free surface $z = h_s(x, y, t)$, we assume stress-free conditions and prescribe the surface temperature and the accumulation ablation rate function,

$$T = T_s(x, y, t), \qquad b_s = b_s(x, y, t), \tag{2.8}$$

where examples for this climate driving are given in [25, 26, 36, 59, 154, 155, 162].

At the *ice-bedrock interface* $z = h_b(x, y, t)$ continuity of temperature and the energy jump conditions must be fulfilled. This implies

$$\chi \frac{\partial T}{\partial n} = \chi_R \frac{\partial T_R}{\partial n}, \qquad T = T_R \tag{2.9}$$

when the base is cold, and

$$b_b = \frac{1}{\varrho_w L_s} \left(\chi \frac{\partial T}{\partial n} - \chi_R \frac{\partial T_R}{\partial n} + \tau^* v_{||} \right), \qquad T = T_R = T_M, \tag{2.10}$$

when it is temperate. In the above, $\mathbf{n}(n)$ indicates the unit vector (direction) normal to and directed into the ground, L_s the latent heat of fusion, $\boldsymbol{\tau}^* \cdot \mathbf{v}_{||}$ the frictional heat due to sliding of the ice sole over the bedrock and $\boldsymbol{\tau}^* = (\boldsymbol{\sigma} - p^* \mathbf{1})\mathbf{n}$ denoting the tangential tractions and $v_{||}$ the jump in tangential velocity. In general, the lithosphere velocity is ignored, so $\mathbf{v}_{||} = -(\mathbf{v} - (\mathbf{v} \cdot \mathbf{n}))\mathbf{n}|_{\text{Ice}}$. Common sliding laws are

$$v_{||} = \begin{cases} \mathcal{C}(|\boldsymbol{\tau}^*|, p^*)\boldsymbol{\tau}^* = c|\boldsymbol{\tau}^*|^{m-1}, p^{*-l}\boldsymbol{\tau}^*, & \text{if} \quad T = T_M, \\ 0, & \text{if} \quad T < T_M, \end{cases} \tag{2.11}$$

according to [112, 137, 178, 182, 183, 185, 187] and with appropriate choices for c, m and l, see [25, 26].

At the *lower boundary of the rock* $z = h_b(x, y)$, we simply prescribe the thermal Neumann condition

$$\chi_R \frac{\partial T_R}{\partial z} = -G, \tag{2.12}$$

where G (≈ 42 mW m^{-2}) (see, however, also [55, 83, 177]) is the geothermal heat flow.

As long as the *ice margin* stays on the continent, we let it freely evolve, either advancing or retreating, depending on whether there is net mass addition or subtraction. When the ice margin reaches the ocean then all mass flowing through that margin position is treated as calving and is lost to the ice sheet. This mechanism is interrupted only when the ice is retreating again at sheet positions distant from the ocean. This is a simplified marginal condition as the formation of ice shelves is ignored. It could be incorporated, see e.g. [9, 58, 60, 83, 84, 85], [121 – 124], if an ice shelf model is adjoined.

2.3. Shallow ice approximation

Ice sheets are long and wide but generally shallow. This suggests to introduce a scaling of the equations of the preceding section such that the aspect ratio $\varepsilon = [H]/[L] \ll 1$, in which $[H]$ and $[L]$ are a typical depth and horizontal distance, explicitly enters the equations, and perturbation methods in the small parameter ε can be used. The lowest order equations of this scheme have been coined the shallow ice approximation [71].

2.3.1. Introduction of scales. In the Cartesian coodinate system x, y (horizontal), z (vertical) we now choose the following scalings:

$$
\begin{aligned}
\{x, y, z, t\} &= \left\{[L]x^*, [L]y^*, [H]z^*, \frac{[L]}{[H]}t^*\right\}, \\
\{u, v, w, b_s, b_b\} &= \{[U]u^*, [U]v^*, [W]w^*, [W]b_s^*, [W]b_b^*\}, \\
\{p, \sigma_x', \sigma_y', \sigma_z', \tau_{xy}, \tau_{xz}, \tau_{xz}\} & \\
&= [\varrho g H]\{p^*, \varepsilon^2\sigma_x^{*\prime}, \varepsilon^2\sigma_y^{*'}, \varepsilon^2\sigma_z^{*\prime}, \varepsilon^2\tau_{xy}^*, \varepsilon\tau_{xz^*}, \varepsilon\tau_{xz}^*\}, \\
T &= T_0 + [\Delta T]T^*, \\
A(T')f(I\!I_{\sigma'}) &= \frac{[D]}{[\sigma]}A^*(T^{*\prime})f^*(I\!I_{\sigma'}^*),
\end{aligned}
\tag{2.13}
$$

where $[L]$, $[H]$, $[U]$, $[W]$, $[\Delta T]$, $[D]$, $[\sigma]$ are length and velocity scales and scales for the temperature range, stretching and typical material stresses. The quantities in brackets are typical values of the variables arising in ice sheets and those with an asterisk are dimensionless and necessarily varying in the range $\mathcal{O}((-1, 1))$, if the bracketed terms are appropriately selected; for typical values see Table 2. The principal assumption of the shallow ice approximation is that

$$
[H]/[L] = [W]/[U] = \epsilon \ll 1\,, \tag{2.14}
$$

anticipated in (2.13) in which several terms are weighted with ϵ and ϵ^2, respectively. This delicate balance introduced here by hindsight, is not obvious and constitutes the essential step towards a formal perturbation procedure obtained independently by HUTTER [67–72] and MORLAND [133, 134].

Table 2. Typical scales of ice sheets.

$[L] = 10^5 - 10^6$ m,	$[\sigma] \approx 10^5$ Pa,
$[H] = 10^2 - 10^3$ m,	$[\varrho] \approx 10$ kg m^{-3},
$[U] = 10 - 10^3$ m a^{-1}	$[g] \approx 10$ m s^{-2},
$[W] = 1 - 10$ m a^{-1}	$[\chi/(\varrho c)] \approx 11.15 \cdot 10^{-6}$ m^2 s^{-1}
$[D] = 1$ a	

With (2.13) and (2.14) the balance laws of mass, momentum and energy and the constitutive relations of stress take the forms

$$
\begin{aligned}
&\frac{\partial u^*}{\partial x^*} + \frac{\partial v^*}{\partial y^*} + \frac{\partial w^*}{\partial z^*} = 0, \\
&\frac{\mathcal{F}}{\epsilon}\frac{\partial u^*}{\partial t^*} = -\frac{\partial p^*}{\partial x^*} + \epsilon^2\frac{\partial \sigma_x^{*\prime}}{\partial x^*} + \epsilon^2\frac{\partial \tau_{xy}^*}{\partial y^*} + \frac{\partial \tau_{xz}^*}{\partial z^*}\,, \\
&\frac{\mathcal{F}}{\epsilon}\frac{\partial v^*}{\partial t^*} = \epsilon^2\frac{\partial \tau_{xy}^*}{\partial x^*} - \frac{\partial p^*}{\partial y^*} + \epsilon^2\frac{\partial \sigma_y^{*\prime}}{\partial y^*} + \frac{\partial \tau_{yz}^*}{\partial z^*},
\end{aligned}
\tag{2.15}
$$

$$
\begin{aligned}
(2.15)\ [\text{cont.}]\quad & \mathcal{F}\epsilon\frac{\partial w^*}{\partial t^*} = \epsilon^2\left\{\frac{\partial \tau^*_{xz}}{\partial x^*} + \frac{\partial \tau^*_{yz}}{\partial y^*}\right\} - \frac{\partial p^*}{\partial z^*} + \epsilon^2\frac{\partial \sigma^{*\prime}_z}{\partial z^*} - 1,\\
& \frac{dT^*}{dt^*} = \mathcal{D}\left\{\epsilon^2\boldsymbol{\nabla}^*_H\cdot(\chi^*_I\boldsymbol{\nabla}^*_H T^*) + \frac{\partial}{\partial z^*}\left(\chi_*\frac{\partial T^*}{\partial z^*}\right)\right\} + \mathcal{E}2A^*(T^*)f^*(\cdot)\mathit{I\!I}^*_{\sigma'},\\
& \frac{\partial u^*}{\partial z^*} + \epsilon^2\frac{\partial w^*}{\partial x^*} = 2\mathcal{G}A^*(T^*)f^*(\mathit{I\!I}_{\sigma'})\tau^*_{xz},\\
& \frac{\partial v^*}{\partial z^*} + \epsilon^2\frac{\partial w^*}{\partial y^*} = 2\mathcal{G}A^*(T^*)f^*(\mathit{I\!I}_{\sigma'})\tau^*_{yz},
\end{aligned}
$$

as well as

$$
\begin{aligned}
(2.16)\quad & \frac{\partial u^*}{\partial x^*} = \mathcal{G}A^*(T^*)f^*(\mathit{I\!I}_{\sigma'})\sigma^{*\prime}_x,\\
& \frac{\partial v^*}{\partial y^*} = \mathcal{G}A^*(T^*)f^*(\mathit{I\!I}_{\sigma'})\sigma^{*\prime}_y,\\
& \frac{\partial w^*}{\partial z^*} = \mathcal{G}A^*(T^*)f^*(\mathit{I\!I}_{\sigma'})\sigma^{*\prime}_z,\\
& \frac{\partial u^*}{\partial y^*} + \frac{\partial v^*}{\partial x^*} = 2\mathcal{G}A^*(T^*)f^*(\mathit{I\!I}_{\sigma'})\tau^*_{xy}
\end{aligned}
$$

in which

$$
\begin{aligned}
\mathit{I\!I}_{\sigma'} &= [\varrho g H]\epsilon^2\left\{{\tau^*_{xz}}^2 + {\tau^*_{yz}}^2 + \epsilon^2\left[\frac{1}{2}\left(\sigma^{*\prime 2}_x + \sigma^{*\prime 2}_y + \sigma^{*\prime 2}_z\right) + {\tau^*_{xy}}^2\right]\right\}\\
&= [\varrho g H]\epsilon^2\mathit{I\!I}^*,
\end{aligned}
$$

$$
\begin{aligned}
(2.17)\quad & \mathcal{F} = \frac{[U^2]}{g[L]},\quad \mathcal{G} = \frac{\epsilon^2}{\mathcal{S}_\Sigma\mathcal{D}_\Delta},\quad \mathcal{S}_\Sigma = \frac{[\sigma]}{\varrho g H},\quad \mathcal{D}_\Delta = \frac{[W]/[H]}{[D]},\\
& \mathcal{D} = \frac{[\chi_I]}{\varrho c_p}\frac{1}{WH},\quad \mathcal{E} = \frac{\mathcal{A}}{\mathcal{S}_\Sigma\mathcal{D}_\Delta},\quad \mathcal{A} = \frac{g[H]}{c_p[\Delta T]}.
\end{aligned}
$$

$\mathcal{F}$ is the Froude number, $\mathcal{S}_\Sigma$ the ratio of deviatoric stress to overburden pressure, $\mathcal{D}_\Delta$ a ratio of mean vertical stretching normalising strain-rate magnitude and $\mathcal{A}$ the energy ratio of gravitational energy to internal thermal energy. $\mathcal{G}$ has the meaning of a dimensionless shear viscosity, while $\mathcal{E}$ measures energy dissipation. Moreover, for Glen's power law, when $(2.2)_2$ is used,

$$
\begin{aligned}
(2.18)\quad & A^* = \exp\left\{-\frac{Q}{RT_0}\frac{1}{1+\dfrac{[\Delta T]}{T_0}T^*}\right\},\\
& f^* = \mathcal{S}\mathit{I\!I}^{*(n-1)/2},\qquad \mathcal{S} := \frac{[\sigma](\epsilon[\varrho g H])^{n-1}}{A_0}.
\end{aligned}
$$

We also have separated the constitutive relations (2.16) from the remaining equations (2.15) because in the lowest order approximation they will not be needed. Similarly, equations (2.3) – (2.12) would also have to be nondimensionalized; however, to motivate the shallow ice approximation, they are not needed.

2.3.2. The limiting theory. Using the scales collected in Table 2 and the definitions (2.17), (2.18) it is seen that $\varepsilon = \mathcal{O}(10^{-2} \div 10^{-3})$, $\mathcal{F} = \mathcal{O}(10^{-8})$ while $\mathcal{G}$, $\mathcal{D}$ and $\mathcal{E}$ are between $\mathcal{O}(1)$ and $\mathcal{O}(10^{-2})$. Thus $\mathcal{F}$ is much smaller than any one of the other dimensionless parameters arising in (2.15) and (2.16), suggesting the Stokes flow limit $\mathcal{F} \to 0$, $\mathcal{F}/\varepsilon \to 0$. The so emerging equations could now be solved by a perturbation expansion $\Phi^* = \sum_{\nu=0}^{\infty} \varepsilon^\nu \Phi_\nu$ for all independent fields $\Phi^* = \{u^*, v^*, w^*, p^*, \sigma_x^*, \sigma_y^*, \sigma_z^*, \tau_{xz}^*, \tau_{yz}^*, \tau_{xy}^*, T^*\}$; however, the shallow ice approximation restricts consideration to the lowest order terms ($\nu = 0$), corresponding to the simultaneous limits

$$\mathcal{F} \to 0, \qquad \mathcal{F}/\varepsilon \to 0, \qquad \varepsilon \to 0. \tag{2.19}$$

Returning back to the dimensional notation, equations (2.15) then reduce to

$$\begin{aligned}
\nabla_H \cdot \mathbf{v}_H + \frac{\partial w}{\partial z} &= 0, \\
-\frac{\partial p}{\partial x} + \frac{\partial \tau_{xz}}{\partial z} &= 0, \\
-\frac{\partial p}{\partial y} + \frac{\partial \tau_{yz}}{\partial z} &= 0, \\
-\frac{\partial p}{\partial z} &= \varrho g, \\
\frac{dT}{dt} = \frac{\partial}{\partial z}\left(\kappa \frac{\partial T}{\partial z}\right) &+ 2EA(T')f(\tau^2)\tau^2, \\
\frac{\partial \mathbf{v}_H}{\partial z} &= 2EA(T')f(\tau^2)\boldsymbol{\tau}
\end{aligned} \tag{2.20}$$

in which $\mathbf{v}_H = (u, v)$, $\nabla_H = (\partial x \partial y)$ and $\boldsymbol{\tau} = (\tau_{xz}, \tau_{yz})$. These are seven equations for the seven unknowns $\mathbf{v}_H$, w, p, $\boldsymbol{\tau}$ and T. They comprise the field equations of the shallow ice approximation.

It turns out that a similar scale analysis for the heat equation in the rock yields

$$\dot{T}_R = \frac{\partial}{\partial z}\left(\kappa_R \frac{\partial T_R}{\partial z}\right), \tag{2.21}$$

while the evolution equations for the free surface (2.4) and the bed (2.5) remain unchanged. Alternatively, the reduced boundary conditions become:

- at the free surface $z = h_s(x, y, t)$

$$p = 0, \qquad \tau_{xz} = \tau_{yz} = 0, \qquad T_s = T_s(x, y, t), \qquad b_s = b_s(x, y, t); \tag{2.22}$$

- at the ice bedrock interface $z = h_b(x, y, t)$

$$\left.\begin{aligned} \chi\frac{\partial T}{\partial z} &= \chi_R\frac{\partial T_R}{\partial z}, \quad T = T_R\,, \\ \mathbf{v}_H &= 0 \end{aligned}\right\} \text{cold ice,}$$

$$\left.\begin{aligned} b_b &= \frac{1}{\varrho_w L_s}\left(\chi\frac{\partial T}{\partial z} - \chi_R\frac{\partial T_R}{\partial z} + \tau^* v_{||}\right), \quad T = T_R = T_M, \\ \mathbf{v}_H &= c|\boldsymbol{\tau}|^{m-1}p^{-l}\boldsymbol{\tau}, \end{aligned}\right\} \text{temperate ice;} \tag{2.23}$$

- at the lower boundary of the rock: $z = 0$

$$\chi_R\frac{\partial T_R}{\partial z} = -G. \tag{2.24}$$

The distinctive features of the shallow ice approximation are the following three points (i)–(iii):

(i) The vertical momentum balance reduces to the cryostatic force balance between vertical pressure gradient and the gravity force. (ii) The horizontal momentum balance comprises force balances between the horizontal pressure gradient and the corresponding vertical gradient of the shear stresses. Together with the boundary conditions $(2.22)_{1,2,3}$, these equations can be integrated to yield the stress fields

$$\begin{aligned} p(x, y, z, t) &= \varrho g(h_s(x, y, t) - z), \\ \boldsymbol{\tau} &= \varrho g(h_s(x, y, t) - z)\nabla_H h_s(x, y, t), \end{aligned} \tag{2.25}$$

which depend on geometry but not on material properties. Provided the temperature distribution is known, $(2.20)_{1,6,7}$ together with (2.25) imply (through integration)

$$\begin{aligned} \mathbf{v_H}(x, y, z, t) &= \mathbf{v_H}(h_b) + C(z, t, \|\nabla_H h_s\|)\,\nabla_H h_s, \\ C(z, t, \|\nabla h_s\|) &= -2\varrho g\int_{h_b}^{z} EA(T_I'(z'))\,f(\tau^2(z'))\,(h_s - z')\,dz', \\ w(x, y, z, t) &= w(h_b) - \int_{h_b}^{z}\nabla_H\cdot\mathbf{v}_H(x, y, z')\,dz', \\ \tau(x, y, z, t)^2 &= (\varrho g(h_s(x, y, t) - z)\|\nabla_H h_s\|)^2, \\ \|\nabla_H h_s\| &= \left(\frac{\partial h_s(x, y, t)}{\partial x}^2 + \frac{\partial h_s(x, y, t)}{\partial y}^2\right), \\ \mathbf{v}_H(h_b) &= \begin{cases} \mathbf{0} & \text{(cold ice)}, \\ -c(\varrho g h)^{m-l}\|\nabla_H h_s\|\nabla_H h_s & \text{(temperate ice)}, \end{cases} \\ w(h_b) &= \mathbf{v}_H(h_b)\cdot\nabla_H h_b\,. \end{aligned} \tag{2.26}$$

It follows that the velocity field within the ice shield can be computed by mere quadratures (if the temperature field and the geometry are prescribed). The formulas $(2.25)_2$ and $(2.26)_{1,6}$, however, also imply the following important facts of the shallow ice approximation, which can be tested by observation and thus may be used as evidence whether the approximation is applicable in a particular case:

- The horizontal shear stress vector points in the direction of steepest descent of the free surface. It is zero parallel to the level lines.

- At any given position in the horizontal plane, the horizontal velocity vector $\mathbf{v}_H$ does not change direction with depth. Its direction at all depths is that of the steepest descent of the surface topography.

- A dome or a trough is the location of vanishing horizontal velocity.

These properties were first recognized by HUTTER [71].

(iii) The heat equation shows that, whereas heat advection is significant in all spatial directions, conduction is dominant in the vertical direction. This means that the heat equation is parabolic only with regard to the vertical coordinate, but has been hyperbolized in the horizontal directions. For very thick ice sheets(2) vertical thermal diffusion is small ($\mathcal{D} \ll 1$) and dissipation large ($\mathcal{E} = \mathcal{O}(1)$) so that thermal diffusion essentially operates only in a near-basal boundary layer. For very thin ice sheets $\mathcal{D} = \mathcal{O}(1)$ and $\mathcal{E} \ll 1$, so vertical convection of heat is significant over the entire depth but dissipation is small. In ice sheet modelling through ice ages both situations must be expected, leaving no room for further simplifications.

This limiting equation set has been used by virtually all numerical modellers who deal in one way or another with the deformation and distribution of temperature in ice sheets. Isothermal plane and axisymmetric [134, 135] flows, thermomechanically uncoupled cases with prescribed temperature [136] and the full plane [35, 61, 62, 78, 102] and axisymmetric [79] coupled cases were analysed before the full three-dimensional theory was numerically implemented in FD-programs [16, 17, 18, 80, 90, 91]. With them the steady-state response of Greenland, Antarctica and other ice sheets were studied, but also their response to climate variations, including complete interglacial cycles [19–23, 59, 81, 82, 84, 86, 87, 88, 89, 103, 105, 125, 129, 158, 188]. Historical and hypothetical ice sheets were also studied [4, 85, 99]. Presently, the physical as well as theoretical weaknesses of this limiting model are recognized; the theory has been extended e.g. to handle polythermal ice [7, 47, 50–56, 68, 71], but the shallow ice approximation is also extended to overcome its mathematical shortcomings.

(2) Compare the definitions of $\mathcal{D}$ and $\mathcal{E}$ in (2.17).

2.4. Limitations of the shallow ice approximation

These occur because the shallow ice approximation is, as an asymptotic theory, not uniformly valid in the entire domain over which the ice extends. Regions of its fallacy are near-margin zones and the vicinity of ice domes and ice divides. Both can be revealed by scrutinizing the ice-thickness-evolution equation (2.4), which upon using (2.5) and (2.26) takes the form

$$\begin{aligned}\frac{\partial h_s}{\partial t} &= \nabla_H\cdot(\mathcal{D}_{sg}\nabla_H h_s) + b_s + b_b - \frac{1}{\tau_l}\left(h_b - h_0 + \frac{\varrho}{\varrho_a}h\right)\\ &= \mathcal{D}_{sg}\triangle_H h_s + (\nabla_H\mathcal{D}_{sg})\cdot\nabla_H h_s + b_s + b_b - \frac{1}{\tau_l}\left(h_b - h_0 + \frac{\varrho}{\varrho_a}h\right),\end{aligned} \tag{2.27}$$

where

$$\begin{aligned}\mathcal{D}_{sg}(h_s, h_b, \|\nabla_H h_s\|) &= \mathcal{D}_s(h_s, h_b, \|\nabla_H h_s\|) + \mathcal{D}_g(h_s, h_b, \|\nabla_H h_s\|)\\ &= c(\varrho g)^{m-l}(h_s - h_b)^{m-l+1}\|\nabla_H h_s\|^{m-1}\\ &\quad + 2\varrho g E\int_{h_b}^{h_s} A(T'(z))f(\tau^2(z))(h_s - z)^2\,dz\\ &\overset{\text{Glen}}{=} c(\varrho g)^{m-l}(h_s - h_b)^{m-l+1}\|\nabla_H h_s\|^{m-1}\\ &\quad + 2(\varrho g)^n E\|\nabla_H h_s\|^{n-1}\int_{h_b}^{h_s} A(T'(z))(h_s - z)^{n+1}\,dz,\end{aligned} \tag{2.28}$$

in which (2.5) has been used and $(2.28)_2$ is valid for a power law fluid. $\mathcal{D}_{sg}$ is a diffusivity with $\mathcal{D}_s$ and $\mathcal{D}_g$ due to sliding and gliding, respectively, and formally $\mathcal{D}_s = 0$ for a cold base. Equation (2.27) is a parabolic advection-diffusion equation for h_s. For $A(T')$ as defined in (2.2) and for a positive-definite creep response function $f(x)$ (> 0 for $x > 0$, $= 0$ for $x = 0$), or for $n \geq 1$ (i.e. Newtonian or pseudoplastic behaviour) the integrals in (2.27) are bounded. The exact margin behaviour depends on the values of m, l and n and could be analysed as shown in [62]. We are satisfied here with a restricted analysis that discloses the difficulties and refer the reader to [44, 71].

2.4.1. Near margin behaviour. The behaviour of D_s, D_g and their gradients in the neighbourhood of the margin as $h_s \to h_b$ depends on the exact functional forms of A, f, on the exponents m, l (and n), as well as on the functional forms of b_s and b_b in the vicinity of the margin. This behaviour can be extracted from a local analysis and it turns out that, when $h_s(x, y, t) \to h_b(x, y, t)$ as the margin is approached, $\|\nabla_H h_s\|$ usually becomes unbounded. A finite marginal slope is only obtained (i) at a cold margin ($\mathcal{D}_s = 0$) when Newtonian behaviour at small

strain rates is permitted (i.e., for a power law with $n = 1$), and (ii) when sliding is permitted close to the margin if $m = 1$. None of these cases is usually assumed – one uses Glen's flow law with $n = 3$ and $m = 3$, $l = 2$ – and so computed margin slopes must be infinite. The detailed analysis of this for plane flow is given e.g. in [44, 62, 71, 134]. Morland and co-workers request the sliding law to be such that finite slope profiles at the margin are obtained in which case uniform validity of the shallow ice approximation is guaranteed, [62, 135, 136, 137]. In numerical implementations of all other authors except [78, 173], the singular marginal behaviour is assumed to be local, not affecting the solution away from it a great deal. All the more, the mesh size is usually considerably larger than the marginal boundary layer is thick; in other words, the numerics determine a finite marginal slope and thus regularize the margin by effectively introducing a mesh-dependent sliding law. Thus, this passive boundary layer does not seem to be a real problem.

2.4.2. Large surface curvature at ice divides. Consider next the vicinity of a dome which is characterized by $\nabla_H h_s = \mathbf{0}$. Thus, according to (2.25) and (2.26)

$$\mathbf{v}_H = \mathbf{0}, \qquad \boldsymbol{\tau} = \mathbf{0}, \qquad \tau^2 = 0 \ \text{(at dome)}.$$

Let us choose the Cartesian coordinate system with origin at the dome. It then follows from (2.26) locally, i.e., at $(x, y) = \mathbf{0}$

$$\nabla_H \cdot \mathbf{v}_H = -\Big\{ c(\varrho g)^{m-l}(h_s - h_b)\, \|\nabla_H h_s\|^{m-1} + 2\varrho g E f(0) \int_{h_s}^{z} A(T'(\bar{z}))(h_s - \bar{z})\, d\bar{z} \Big\} \triangle_H h_s \tag{2.29}$$

and from (2.4)

$$\frac{\partial h}{\partial t} + \int_{h_b}^{h_s} \nabla_H \cdot \mathbf{v}_H \, dz = b_s + b_b. \tag{2.30}$$

Combining (2.29) and (2.30) yields

$$\frac{\partial h}{\partial t} - \mathcal{D}_0 \triangle_H H = b_s + b_b \qquad \text{(at dome)}, \tag{2.31}$$

where $\mathcal{D}_o = \mathcal{D}_s + \mathcal{D}_{g_0}$ is defined in (2.28) and $\mathcal{D}_{g_0}$ is obtained from $\mathcal{D}_g$ by replacing $f(\tau^2)$ by $f(0)$ (which for Glen's flow law equals zero). In steady state (2.31) can be used to evaluate the mean surface curvature at the ice divide,

$$\triangle_H h_s = \frac{b_s + b_b}{\mathcal{D}_s + \mathcal{D}_{g_0}} \qquad \text{(at dome)}, \tag{2.32}$$

which explains why the shallow ice approximation may fail close to divides. Indeed, at a cold divide $\mathcal{D}_s = 0$ and otherwise $\mathcal{D}_s = 0$ unless $m = 1$. Furthermore, when $f(0) = 0$, $\mathcal{D}_{g_0} = 0$ as well, implying that $\triangle_H h_{s\,\mathrm{dome}} = \infty$ in this case, in violation with the shallowness assumption. Since basal sliding cannot be guaranteed at a dome, regularization of the kinematic surface equation at least requires a finite viscosity flow law ($f(0) \neq 0$). However, even with this incorporated, very large surface curvatures must be expected at a divide.

As was done for the margin regions, numerical integration can be performed and the divide zone formally regularized through discretization, however observations indicate that near-divide velocities and temperatures are not accurate in general.

In attempts to date the ice from ice cores in connection with isotope composition studies [1, 2, 3, 11, 12, 13, 93–101, 118, 119, 120, 157, 169–172], the necessity of incorporation of "longitudinal stresses" was recognized, but computations [28–31, 160, 161, 163, 166, 167] employ streamline models and steady state with diverging flow properties taken into account by a fudge factor. In short, the computational suggestions are *ad hoc*, not in conformity with a proper scaling, and not appropriate to the three-dimensional situation. First attempts at a systematic use of higher order terms in the perturbation expansion are due to BLATTER [6] and MANGENEY *et al.* [126–128]. Equations (2.15) and (2.16), however, clearly indicate how the shallow ice approximation can be improved either by formal perturbation expansion or iteration. This analysis is presently under way in a dissertation at TH Darmstadt.

3. Application of the model to the Greenland Ice Sheet

The above SIA equations have been computationally solved by using finite difference techniques by BUDD *et al.* [16, 17, 20], CALOV and HUTTER [25, 26], HUYBRECHTS *et al.* [80–89, 103] and FABRÉ *et al.* [36]. These programs are formidable undertakings; we shall not discuss their peculiarities. We present some computational results obtained with our model, the intention being to highlight the geophysical implications rather than to expose the numerical complexities.

Ice sheet dynamics is governed by external and internal parameters; the first contribute to their driving, the second affect their response. The most important external driving parameters are furnished by the implemented atmospheric model of which a very simple version will be presented. Other less direct external "forcings" are the interaction of the ice sheet with the solid earth through the geothermal heat, the bedrock sinking and through the handling of the calving mechanism at ocean boundaries. Internal parameters relate to the material behaviour, here most conspicuously expressed by the enhancement factor, the sliding law at the ice-bed interface and the dissipation associated with it.

We shall in this section describe these couplings and present some parameter studies using the Greenland Ice Sheet as a test case. Then simplified climate scenarios will be applied and, finally, a comparison of the computed with the measured velocity transect – the so-called EGIG line – will be made. These comparisons will not only delineate the difficulties that one encounters when trying to identify phenomenological parameters of such a large geophysical system, but equally demonstrate the sheer impossibility of achieving an objective comparison.

3.1. Simplified model-atmosphere

In the model, the *atmospheric surface temperature* will be prescribed in the form

$$T_a(x,y,t) = T_a(x,y)|_{\text{loc}} + T_D(t), \tag{3.1}$$

where $T_a(x,y)|_{\text{loc}}$ is the present local distribution of the mean atmospheric temperature, and $T_D(t)$ describes the long periodic climate changes. For Greenland, data of the local temperature was collected by OHMURA [154] and very well fit by the linear relation $T_a|_{\text{loc}} = \vartheta_0 + a_0\varphi + \gamma h_s$, $\vartheta_0 = 55.76$ [°C], $a_0 = -0.8471$ [°C °North^{-1}], $\gamma = -8$ [°C km^{-1}], in which φ is latitude and h_s surface height above sea level. $T_D(t)$ is the climate driving and will be selected according to which climate scenario is modelled.

The *accumulation-ablation-rate fuction*

$$b_s = S - M \qquad [\text{m a}^{-1}, \quad \text{ice equivalent}] \tag{3.2}$$

is divided into *snowfall* S and *melting* M. The present-day annual mean of the snowfall is represented as a polysurface deduced from data reported by OHMURA and REEH [155]; the annual mean snowfall at earlier times is modelled according to

$$\begin{aligned} S(t) &= S_{\min} + (S_{\text{today}} - S_{\min})\frac{T_D(t) - T_D^{\min}}{T_D^{\text{today}} - T_D^{\min}}, \\ S_{\min} &= 0.5\, S_{\text{today}}, \qquad T_D^{\min} = -10^\circ\text{C}, \qquad T_D^{\text{today}} = 0^\circ\text{C}. \end{aligned} \tag{3.3}$$

This assumes that the snowfall was half as large at the climate minimum as it is today.

To parameterize the melting, we employ BRAITHWAITE'S [10] "positive degree day" formula

$$M = \frac{\beta_2}{Y}\max\left(0, \Sigma_+ - \frac{P_{\max} Y}{\beta_1} S\right) \tag{3.4}$$

with

$$\Sigma_+ = \begin{cases} YT_a & T_A \le T_a, \\ \dfrac{Y}{\pi}\left(T_a \arccos\left(-\dfrac{T_a}{T_A}\right) + \sqrt{T_A^2 - T_a^2}\right) & -T_A < T_a < T_A, \\ 0 & -T_A \ge T_a, \end{cases}$$

$$\beta_1 = 0.9\,, \qquad \beta_2 = 2.6 \qquad [\text{m water equivalent a}^{-1}\,^{\circ}\text{C}^{-1}],$$
$$Y = 10\,\text{a}\,, \qquad P_{\max} = 0.6,$$

which accounts for the percolation and re-freezing of melt-water and superimposed ice, respectively. T_a is the mean annual air temperature and T_A its seasonal amplitude. For a detailed explanation, see CALOV and HUTTER [26].

3.2. Handling of the model ice margin

As long as the ice margin stays on the continent we let it freely evolve, either advancing or retreating, depending on whether there is net mass addition or subtraction. When the ice margin reaches the ocean, then all mass flowing through that margin position is treated as *calving* and is lost to the ice sheet. This mechanism is interrupted only when the ice is retreating again at sheet positions distant from the ocean.

In the simulations described below, the sea level will be held constant; however in more realistic modelling it should be a function of time.

3.3. Computations of ice thickness distribution under steady driving conditions

3.3.1. Variation of the amplitude of the annual temperature. We present here the results of computations of the steady-state geometry of the Greenland Ice Sheet subject to various external time-independent driving conditions. The model is integrated subject to various parameterizations, using today's ice thickness distribution and temperature distribution it obtains for today's thermal equilibrium as initial conditions. Computations are continued until the ice thickness and the ice margins as well as the temperature distribution no longer change. This happens at approximately 50 000 model years. In the standard run we use as geothermal heat $G = 42$ mW m^{-2}, as enhancement factor $E = 3$, and as seasonal air temperature amplitude $T_A = 14^{\circ}$C. Figure 2 a displays the level lines of the free surface and the ice margins obtained when also the no-slip condition is imposed on the entire basal surface. When compared to the observed present surface topography (see CALOV and HUTTER [26]), the ice extends too far to the North and does not extend enough in the South. Moreover, the computed Summit height is about 600 m too high.

If we enlarge or lower the amplitude of the annual temperature variation by 7°C, to $T_A = 21^{\circ}$C (Fig. 2 b) and $T_A = 7^{\circ}$C (Fig. 2 c), it is seen that the former results in a substantial ice sheet reduction while the changes in the latter scenario are far less dramatic. This non-symmetry in the behaviour is due to the boundary conditions at the ice-ocean margin: free evolution for ice retreat but full calving for advance.

3.3.2. Variation of the sliding parameter. By incorporating a sliding condition along the ice-bedrock interface, reduced ice thickness (close to reality) can be modelled; this is simply because ice flows more easily toward the margins. At

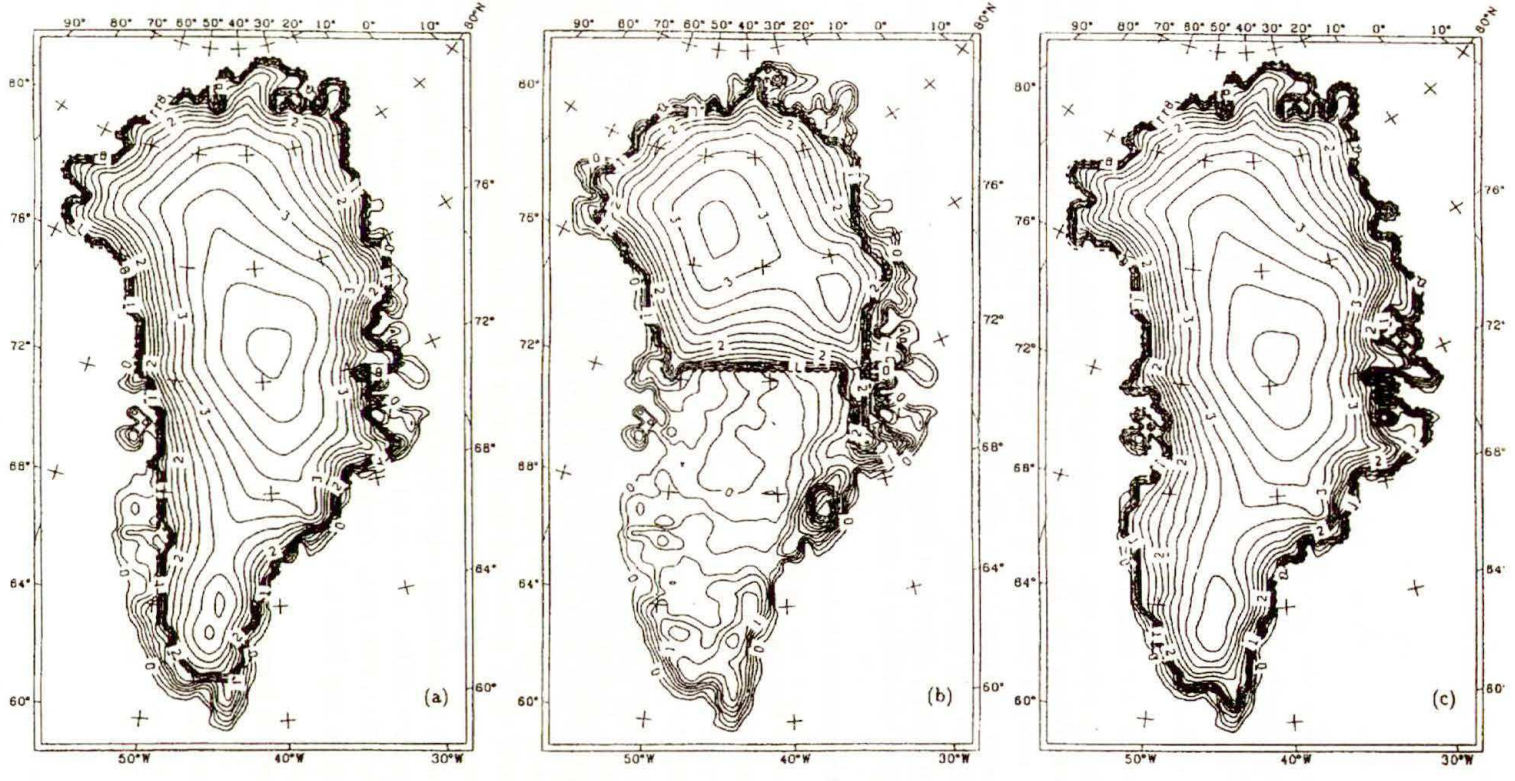

FIG. 2. Level lines of the free surface of the Greenland Ice Sheet (equidistance 200 m) for the steady-state computations under present conditions with the enhancement factor $E = 3$ using the amplitude of annual temperature $T_A = 14°C$ (a), $T_A = 21°C$ (b) and $T_A = 7°C$ (c).

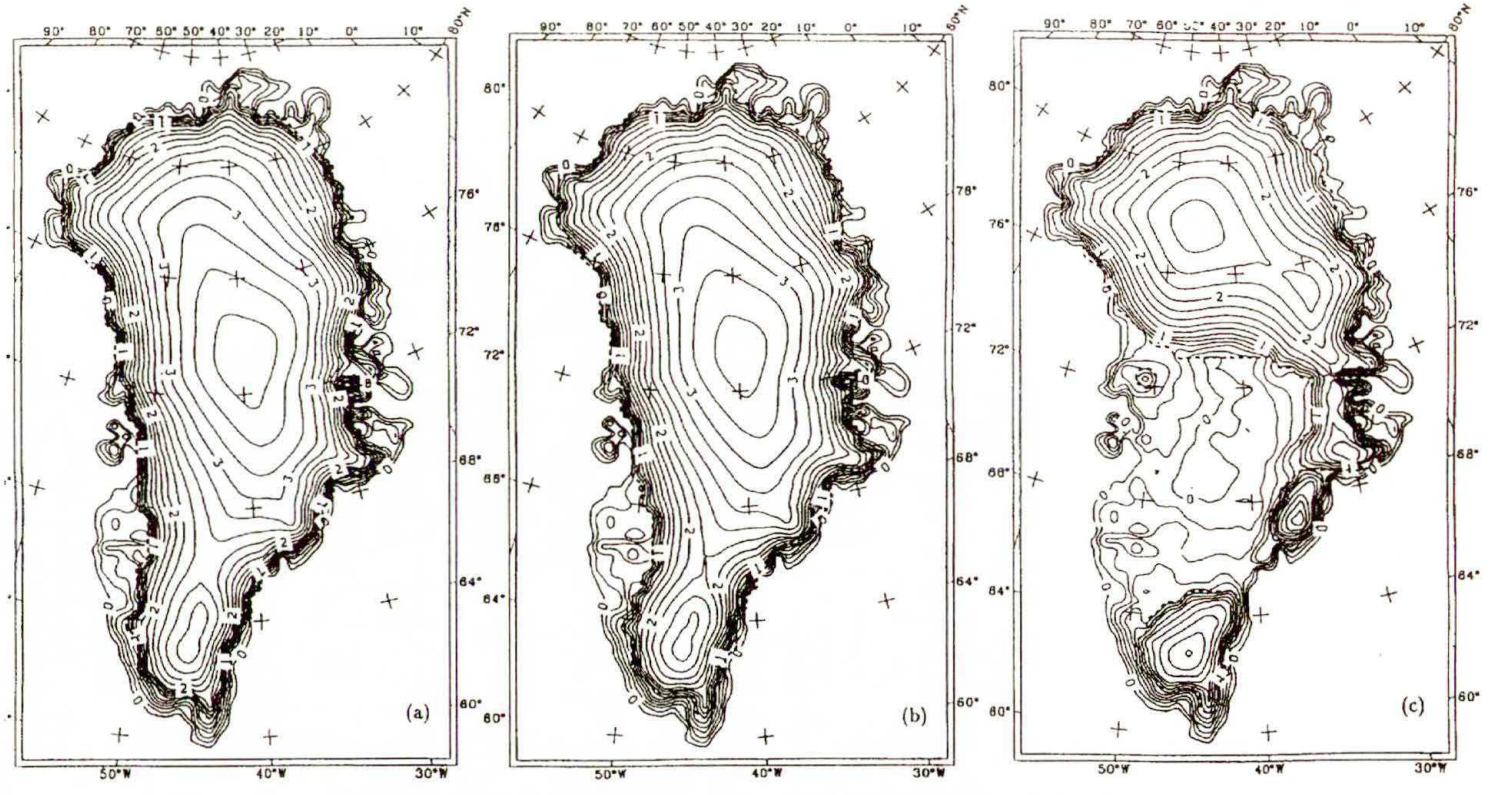

FIG. 3. Level lines of the free surface of the Greenland Ice Sheet in present steady-state using a latitude-dependent amplitude of temperature and incorporating sliding in the entire basal area with a sliding parameter $c_M = 2 \times 10^4\,\mathrm{a}^{-1}$ (a), $c_M = 6 \times 10^4\,\mathrm{a}^{-1}$ (b) and $c_M = 10 \times 10^4\,\mathrm{a}^{-1}$ (c).

a positive feedback margin slopes will be less steep and there is an increased ablation zone.

We shall use the sliding law

$$\mathbf{v}_H(h_b) = -c_M h \|\nabla_H h_s\|^2 \nabla_H h_s \,, \tag{3.5}$$

in which h is the ice thickness and h_s the surface height a.s.l. ∇_H is the horizontal gradient operator, $\mathbf{v}_H$ the horizontal velocity and c_M a coefficient with dimension a^{-1}.

Computations were performed for steady state using now a latitude-dependent amplitude of annual temperature $T_A = a + b\varphi$, $a = -23°\mathrm{C}$, $b = 0.55°\mathrm{C\,North}^{-1}$, and implementing sliding everywhere according to (3.5) with $c_M = (2;\ 6;\ 10) \times 10^4\,\mathrm{a}^{-1}$, and frictional heat due to sliding ignored, Figs. 3 a, b, c. It is seen that increasing the sliding coefficient causes a lowering of the North- and South domes of about 200 m, compare Fig. 3 a with Fig. 3 b. The results for $c_M = 10 \times 10^4\,\mathrm{a}^{-1}$ (Fig. 3 c) are obviously very unrealistic, but they demonstrate how catastrophically an ice sheet can develop when sufficient sliding is provided. The ice sheet has been split into essentially two parts with an ice-free 800 km wide zone in Middle-Greenland. The South cap exists, because it sits on high elevated ground but equally also because of the large snow accumulation rate there. If the frictional basal heat were incorporated, the two caps in Fig. 3 c would be even smaller; however, rebound of the substratum is a negative feedback and both may approximately balance.

Scenarios with sliding restricted to the basal melting zones, and frictional heat as well as bedrock sinking incorporated are analysed by WEIS *et al.* [188].

3.3.3. Variation of other parameters. We have also varied the snow melting parameters β_1, β_2 and the geothermal heat. While these also have some definite influences upon the steady-state geometry of an ice sheet, their variation about the most realistic values has indicated less dramatic sensitivity than with variations of the amplitude of the mean annual temperature T_A or the sliding coefficient c_M. However, variations in the geothermal heat flow changes the temperature distribution close to the base considerably.

3.4. Basal temperature evolution through the ice age

3.4.1. Glacial climate cycles. The external driving surface temperature T_D is constructed from the data of the Vostok ice core, Antarctica (BARNOLA *et al.* [1]), by selecting upper and lower bounds, Fig. 4,

$$T_D(t) = \begin{cases} T_D^{\mathrm{I}}(t) & \text{climate I,} \\ T_D^{\mathrm{II}}(t) & \text{climate II,} \end{cases} \tag{3.6}$$

respectively. These idealized cycles are prolonged by one period into the past in order that the model can be spun-up to appropriate initial conditions at the

end of the Illinoian Ice Age. The idealized climates I and II reproduce the steep warming from the climate minima to the interglacials very well, but model the slower decay from the Eemian Interglacial to the Wisconsin minimum relatively poorly. We thus expect different results for the two.

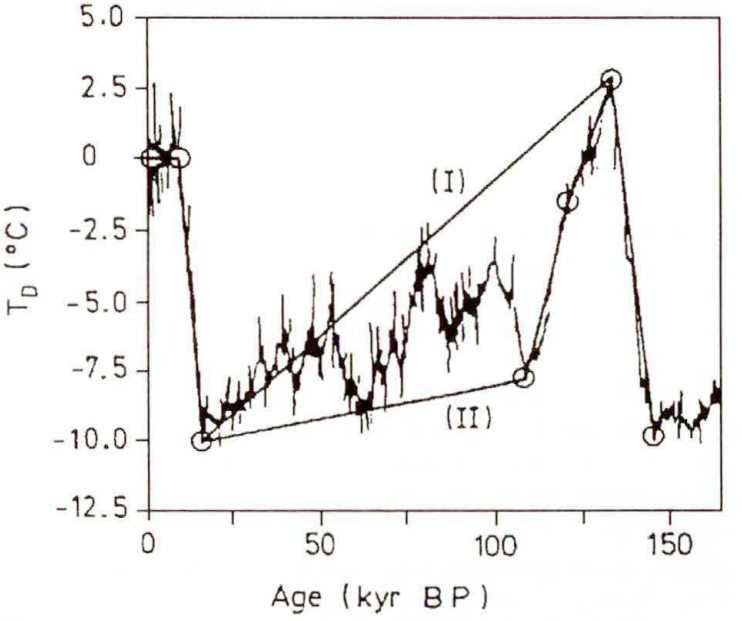

FIG. 4. Vostok δD-temperatures as taken from BARNOLA *et al.* [1] from present to 160 ka BP together with the model climate scenarios (I) and (II) that describe an approximate upper and lower bound to the Vostok data. Circles indicate points with abrupt climate changes or at climate maxima and minima, respectively.

Computional results are presented for the following scenarios:

• I or II: Response of the Greenland Ice Sheet under standard conditions (i.e., $E = 1$, $G = 42$ mW m^{-2}, no-slip) to the external climates I and II, respectively, while ignoring the thermal response of the substrate.

• I-S: Same as I, but now the response of the substrate is taken into account.

• I-S-E=3: Same as I-S, but now the enhancement factor of Wisconsinan ice is applied throughout.

In the first set of computations the ice thickness distribution will be held constant, the intention being to isolate the thermal response of the system substrate-inland ice. If the evolution of the geometry were varied, it would be very difficult to find the primary cause for the particular behaviour.

3.4.2. Basal temperatures at Dye 3, Summit and Camp Century. We discuss here the time series of temperature at the base which follow from computations according to the above idealized climate scenarios. The time series should not be

regarded as giving a realistic temperature distribution through 275 ka, but they disclose very significant behaviour that could not so well be identified with more realistic scenarios. The bore-hole positions are significant because extensive isotope studies have been performed (HANSEN and LANGWAY [57], DANSGAARD *et al.* [32], JOHNSEN *et al.* [92]). For these analyses it is of interest to know (i) how basal-temperature peaks lag behind the driving peaks, and (ii) whether the basal ice at these positions has at any time been at melting. Keeping the ice geometry fixed puts the results on the safe side in this regard, i.e., makes the base somewhat warmer.

For Dye 3, Summit and Camp Century time series are presented for the driving surface temperature (climate I), the homologous basal temperature of scenarios I, I-S and I-S-E=3, and the deviation of the geothermal heat flow into the ice from the "equilibrium" value $G_{\text{eq}} = 42\ \text{mW m}^{-2}$ of scenarios I-S and I-S-E=3. The sytem is driven by two ice age cycles as illustrated in Fig. 4, lasting from 275 ka BP to present.

a. Dye 3. Scenario I, computed without taking the thermal response of the rock bed into account and by using $E = 1$ (Fig. 5 b) shows that both maxima and minima of the homologous temperature at the base occur 11.6 ka, 6.5 ka and 3.2 ka, respectively, after the corresponding maxima of the driving time series $T_a(t)$. The second of the two phase lags of the minimum is smaller than the first because the temperature rise to the Holocene is faster than that to the Eemian Interglacial. The graph also shows that no spin-up is needed for this scenario, because the two maxima of the basal temperatures are the same. Today's basal temperatures are by 0.5°C lower than the present equilibrium temperature would be. Whereas the deviation of the basal homologous temperature from its corresponding equilibrium value is largest at the last Interglacial (at about 135 ka BP), this deviation is smallest at the climatic minimum.

If the thermal inertia of the rock bed is included (Fig. 5 c), the present homologous basal temperature is 1.69°C below the corresponding equilibrium value. The deviation from the equilibrium value at all times where it is calculated is here larger than for scenario I. The model is not completely spun-up after one cycle because the relative maximum at 110.2 ka BP is larger than that at 237.8 ka BP: The rock layer adds additional thermal inertia to the system. Furthermore, whereas the phase shifts of the minima (6.5 and 3.2 ka) are exactly the same as those of scenario I, those of the maxima are roughly doubled. Interesting to note is the temporal variation of the heat flow into the ice from the rock bed. Panel e) shows the deviation of this flow from its value at the lower boundary, $G_{\text{eq}} = 42\ \text{mW m}^{-2}$. This heat flow is either larger or smaller than its equilibrium value by up to 21%. The present value is by $4\ \text{mW m}^{-2}$ smaller than G_{eq}, and the tendency is falling. Also interesting is that the phase shifts of the maxima (and minima) differ from those of the temperatures. This is the manifestation of nonlinear effects.

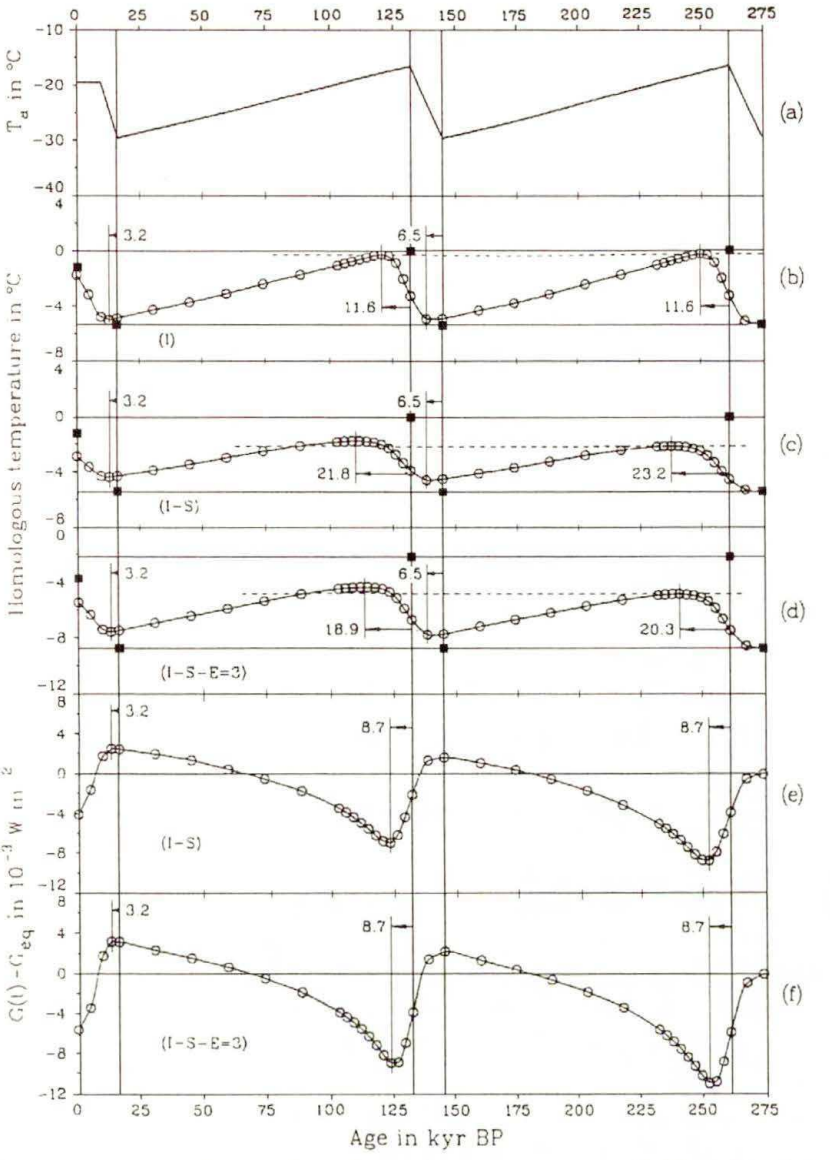

FIG. 5. "Dye 3": Variation of the athmosphere temperature $T_a(t)$ at Dye 3 from today to 275 kyears BP (a), basal homologous temperature for scenarios I (b), I-S (c), I-S-E=3 (d) and the difference of the actual heat flow through the ice-rock interface from the equilibrium value $G_{eq} = 42\,\mathrm{mW\,m^{-2}}$ for scenarios I-S (e) and I-S-E=3 (f). Symbols ○ are computed, solid lines interpolated. ■ mark computed equilibrium values of the homologous basal temperature if the climate were driven with the air temperature at that time. Inserted numbers with arrows show shifts between the relative maximum of the driving temperature and that of the basal homologous temperature or the corresponding minima of the heat flow. The dashed line marks the first relative maximum and compares it with the second.

Computations for a I-S-E=3 scenario, see Fig. 5 d, f, show that, because the ice is softer in this case, cold ice will be transported downward faster than with $E = 1$. Basal temperatures are now colder (by approximately 2°C), and phase shifts of the maximum basal temperatures shorter than for $E = 1$ (20.3 ka, 18.9 ka) while those of the minima remain the same. The variation of the heat flow through the ice-rock interface is also slightly enhanced. Thus the softness of the ice has a significant effect on the thermal regime of the Greenland Ice Sheet through time.

Calculations were also performed for scenario II (without a rock layer and for $E = 1$), but are not shown here. When compared with the results obtained with scenario I it is seen that the faster approach from the Eemian Interglacial to the Wisconsinan minimum is also visible in the temporal distribution of the basal temperature: The base is generally colder than for scenario I, but the maxima and minima of the homologous temperatures and their phase shifts are not very much different from those of scenario I, and, in particular, the present basal temperature is practically the same. The steep warming of the climate at the end of the last Ice Age seems to hide the detailed variations of the climate during the Ice Age.

b. Summit. Let us compare the results for this location with depth $h \approx 3200$ m (Fig. 6) with those of Dye 3, $h \approx 2000$ m. Again the phase shifts between the maxima of the homologous temperature are larger than those of the minima (Fig. 6 b, c, d). For scenario I one glacial cycle is enough to obtain the spun-up temperature distribution. Phase shifts of the maxima of the homologous basal temperature are far larger for scenario I-S than for scenario I. And for softer ice, $E = 3$, the basal temperature and phase shifts are generally smaller than for the corresponding computations with $E = 1$. The heat flow into the ice roughly agrees with the equilibrium value 42 mW m^{-2} but the tendency is falling. All phase shifts for Summit are larger than for Dye 3, and the corresponding amplitudes are smaller, both effects that are largely due to the larger thickness of the ice at "Summit".

c. Camp Century. Because the ice at Camp Century with its 1.4 km thickness is thinnest in comparison to the previous bore hole sites, it is expected that the corresponding phase shifts are smallest and the amplitudes largest, see Fig. 7. Whereas this is indeed so for the amplitudes, the phase shifts for Camp Century are in almost all scenarios and cases as large as (or even larger than) for Dye 3. Note that the phase shift for the first minimum in scenario I-S is larger than for Dye 3. A possible explanation could be that the model is still in the process of spin-up. On the other hand, the result indicates that thickness cannot be the only quantity that is responsible for the delay of basal processes from their climate forcing. Diffusion, advection and dissipation equally contribute. Among the three locations, the temporal variation of the heat flow into the ice deviates most from the equilibrium heat flow, and the present value is smaller than the equilibrium value by an amount of 6 – 8 mW m^{-2}.

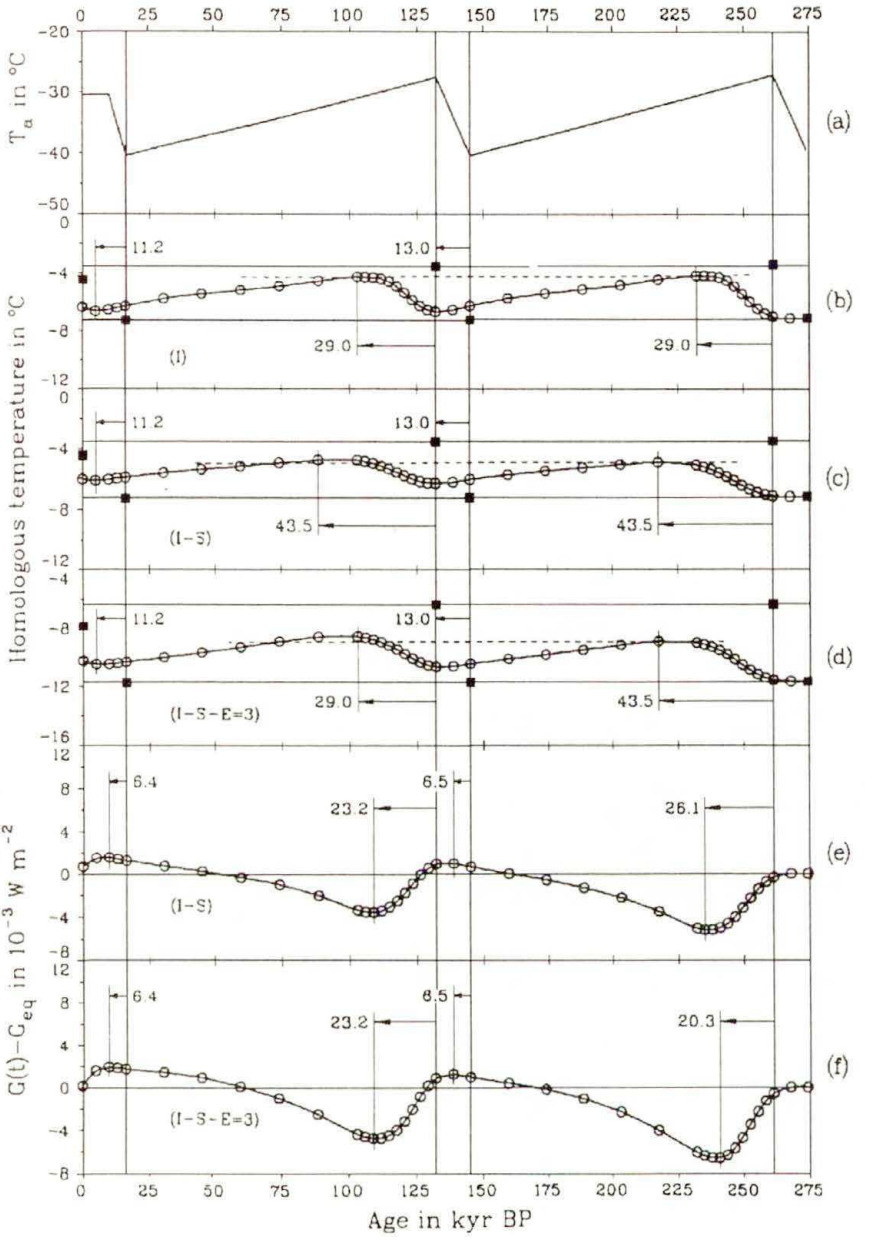

FIG. 6. "Summit". Same as for Fig. 5.

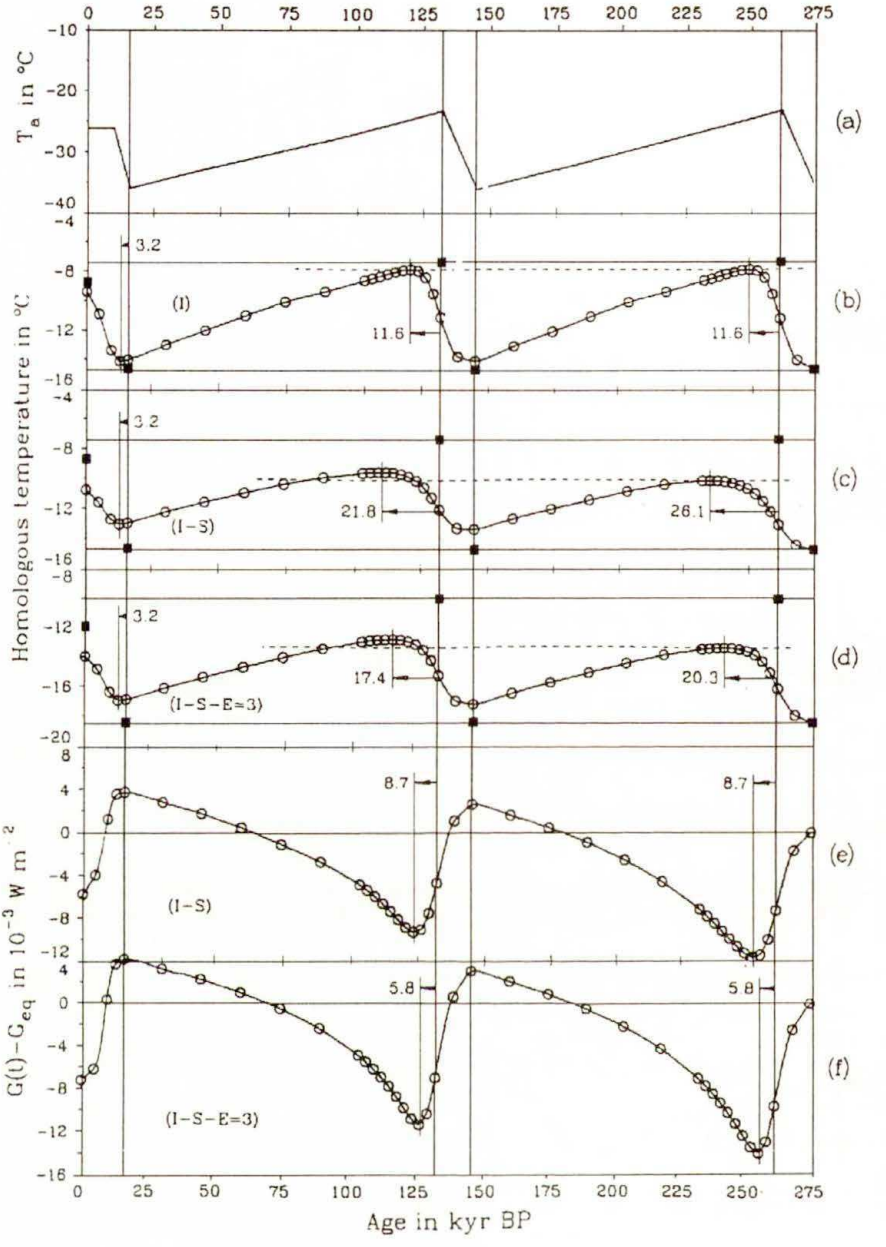

FIG. 7. "Camp Century". Same as for Fig. 5.

3.5. Comparison with the data

In this section we compare the ice-sheet-surface velocities that were measured along the EGIG (International Glaciological Greenland Expedition) traverse [64, 25].

3.5.1. The velocity data along the EGIG traverse. The EGIG traverse is the best known measuring traverse in Greenland and crosses Greenland approximately at the 70° N latitude from West to East (see Fig. 8). For our comparison, those measuring points listed in HOFMANN [64] with an approximate distance of 40 km will be considered, which corresponds to our numerical horizontal grid resolution. During the EGIG expedition the free surface velocity

$$v_H^{\text{meas}}(h_s) = |\mathbf{v}_H^{\text{meas}}(h_s)| = |v_x^{\text{meas}}(h_s)\mathbf{e}_x + v_y^{\text{meas}}(h_s)\mathbf{e}_y| \tag{3.7}$$

and the polar angle Θ^{meas} between the vectors $\mathbf{e}_x$ and $\mathbf{v}_H^{\text{meas}}$ were measured. Figure 8 displays the measured EGIG velocities (i.e. horizontal projections) as arrows at positions P 1 to P 17 along with the level lines of the free surface topography. These velocities decrease from $109.71\,\text{m}\,\text{a}^{-1}$ at position P 1 in the West to a minimum of $3.54\,\text{m}\,\text{a}^{-1}$ at position P 14 in the center and increase again to $12.46\,\text{m}\,\text{a}^{-1}$ at position P 17 in the East. Qualitatively, this is in conformity with the shallow ice approximation, which states that the horizontal velocities are pointing in the direction of steepest descent (i.e., orthogonally to the level lines) and are proportional to $(\partial h_s/\partial\sigma)^n$, where σ is the distance measured along the direction of steepest descent and $n = 3$ is the exponent in Glen's power law. Thus the velocities grow with increasing surface slope, corresponding to a reduction of the distance between the level lines, as shown.

3.5.2. Comparison of measured with computed EGIG-velocities using computations with fixed surface geometry. Table 3 summarizes the comparison of the measured and computed surface velocities along the EGIG traverse at points P 1 to P 17 as obtained with climate scenario I-S. This scenario drives the ice sheet evolution with an upper bound of the Vostok temperature data as explained in Sec. 3.4.1. The thermal inertia of a 4 km thick solid rock layer is accounted for and the no-slip condition at the ice-bedrock interface is applied. The enhancement factor in the flow law is $E = 1$ (i.e. Holocene ice conditions are applied throughout), and the geothermal heat is $G = 42 \times 10^{-3}\,\text{W}\,\text{m}^{-2}$. Columns 1, 2 and 3 of Table 3 list, respectively, the measuring point, the modulus of the horizontal components of the free surface velocity $v_H^{\text{meas}}(h_s)$ and its polar angle Θ^{meas} as inferred from the measurements. The corresponding quantities $v_H^{\text{mod}}(h_s)$ and Θ^{mod} are obtained from the computation and listed in Columns 4 and 5. In addition, Table 3 contains in columns 6 and 7 the relative deviations

$$\Delta A_r(h_s) = \frac{v_H^{\text{meas}}(h_s) - v_H^{\text{mod}}(h_s)}{v_H^{\text{mod}}(h_s)} \times 100 \text{ in } \% \tag{3.8}$$

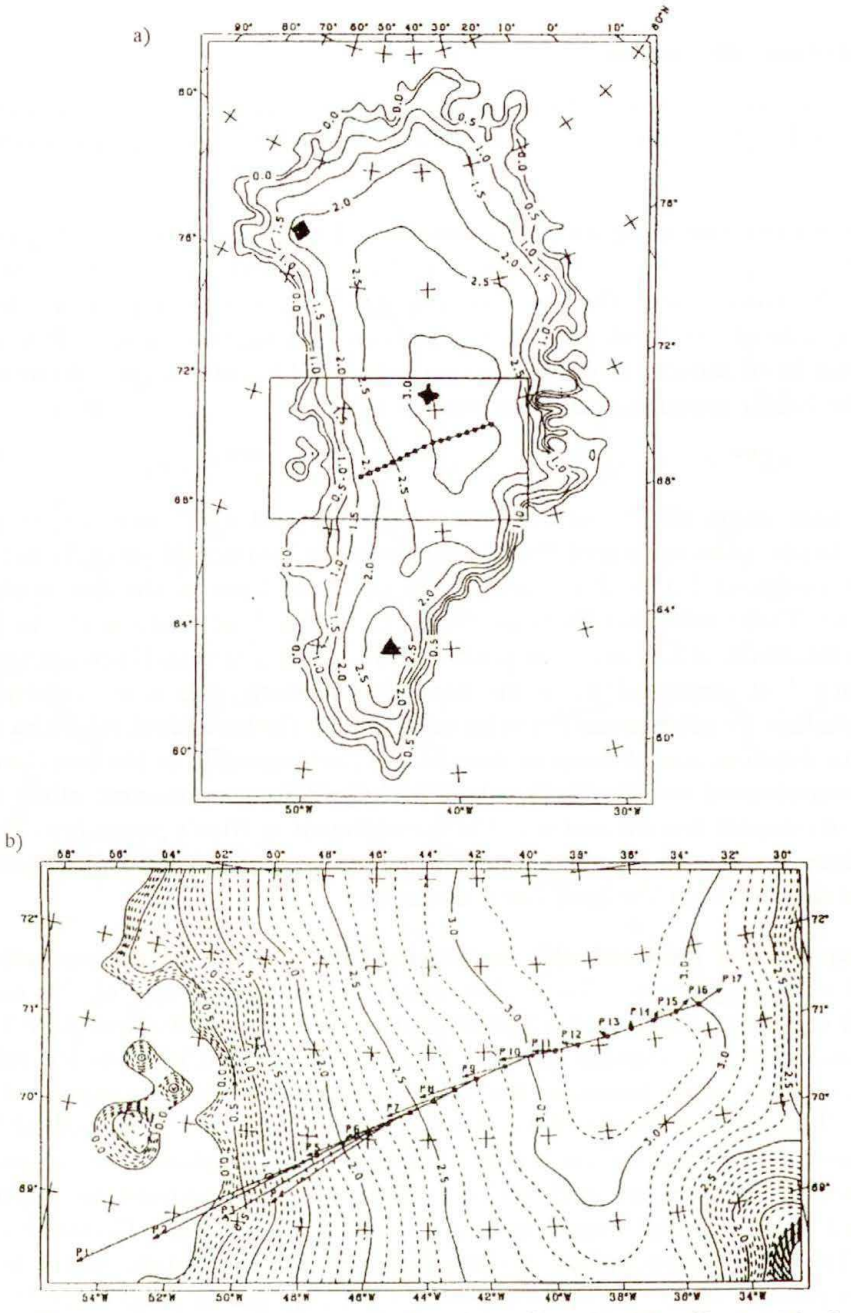

FIG. 8. Present surface topography of the Greenland Ice Sheet with the EGIG-traverse (a). The deep borehole positions are also indicated by a triangle (Dye 3), an asterisk (Summit) and a diamond (Camp Century). Measured velocity vectors at positions P 1 to P 17 along the EGIG-traverse (b) where the comparison with computational velocities is performed, see Tables 3 to 5.

of the measured and modelled EGIG-velocities, and the absolute deviations

$$\Delta\Theta = \Theta^{\text{meas}} - \Theta^{\text{mod}} \tag{3.9}$$

of the modelled from the measured polar angle.

Table 3. Comparison between measured and modelled EGIG-velocities as obtained for conditions of scenario I-S. Columns 1 to 7 list the position, measured surface speeds in $\mathrm{m\,a^{-1}}$, their polar angle in °, the modelled surface speeds and their polar angles and the relative error of the speeds in % and the absolute error in orientation as defined in (3.8) and (3.9).

Position	$v_H^{\text{meas}}(h_s)$ $[\mathrm{m\,a^{-1}}]$	Θ^{meas} [°]	$v_H^{\text{mod}}(h_s)$ $[\mathrm{m\,a^{-1}}]$	Θ^{mod} [°]	$\Delta A_r(h_s)$ [%]	$\Delta\Theta$ [°]
P 1	109.71	203.14	24.42	196.88	349	6.26
P 2	88.28	206.34	26.75	200.33	230	6.01
P 3	70.71	209.91	23.91	201.45	196	8.46
P 4	59.07	213.35	22.32	201.94	165	11.41
P 5	47.75	202.40	17.06	203.82	180	−1.42
P 6	39.96	202.17	13.60	199.39	194	2.78
P 7	31.40	200.60	11.59	202.18	171	−1.58
P 8	25.67	197.76	9.56	202.02	169	−4.26
P 9	18.76	194.73	6.93	200.83	171	−6.10
P 10	13.38	189.73	4.99	200.55	168	−10.82
P 11	9.88	182.79	3.50	200.03	182	−17.24
P 12	6.99	172.80	2.21	196.36	216	−23.56
P 13	4.21	144.46	0.71	190.05	493	−45.59
P 14	3.54	95.56	0.24	39.42	1375	56.14
P 15	4.83	62.10	1.29	24.64	274	37.46
P 16	7.58	44.47	2.87	22.89	164	21.58
P 17	12.46	33.73	4.50	17.42	177	16.31

Today's EGIG velocities of scenario I-S are all smaller than those of the measurements. This must certainly be in part due to the reduced deformability of the model ice with $E = 1$ that corresponds to Holocene conditions. In spite of this, a discussion of the results from scenario I-S reveals useful insight. Qualitatively, the EGIG velocities of scenario I-S show the right dependence on the position along the EGIG traverse. The relative minimum of the modelled velocities arises at position P 14, as in the observations. The computed velocities grow from position P 14 in both directions towards the ice margins in the West and the East. Overall the relative deviation $\Delta A_r(h_s)$ of the modelled from the observed EGIG-velocities is rather large. At position P 1, $\Delta A_r(h_s) = 349\%$; at P 8 it has a low of $\Delta A_r(h_s) = 169\%$ and at position P 14 it is as large as 1375%

(note that if $\Delta A_r(h_s)$ were normalized with $v_H^{\text{meas}}(h_s)$, this value would be 95%; so the discrepancy is highly exaggerated). The best agreement of the modulus of the velocity is reached at P 16 with $\Delta A_r(h_s) = 164\%$. The dependence of the relative velocity deviations $\Delta A_r(h_s)$ on the position of the EGIG-traverse is conspicuously correlated with the free surface height. The latter assumes at P 14 a relative maximum. In addition, in the vicinity of P 14, the gradient of the free surface is rather small. Therefore, there are two explanations for the large deviations of the measured from the computed velocities at P 13, P 14 and P 15. First, the shallow-ice approximation is an invalid approximation in the vicinity of a dome or ice divide and fails at the ice divide when a power flow law is used [44, 78, 71, 133, 159, 161, 173]. Second, small slopes of the free surface means that the numerical determination of these slopes from the height distribution requires the difference between two nearly equal numbers with consequent round-off error, and in turn the propagation of large errors in the evaluation of the velocities.

Overall, the differences $\Delta\Theta$ of the modelled and measured polar angles are not particularly large; this comes as no surprise, because in scenario I-S the smoothed surface topography is prescribed and held fixed during integration. This smoothed topography nearly agrees with the original topography provided by the data. Particularly small values of $|\Delta\Theta|$ arise at P 5, P 6, P 7 and, not surprisingly, the largest values of $|\Delta\Theta|$ occur close to the ice divide at P 14 ($\Delta\Theta = 56.14°$).

The EGIG-velocities, modelled with scenario I-S-E=3 – the computation equivalent to I-S but with an enhancement factor $E = 3$ – show the same qualitative behaviour as do those that were compared for scenario I-S. One would expect roughly a tripling of the modelled velocities; however, because of the thermomechanical coupling, the enlargement of the velocities is somewhat smaller because the basal ice is also colder. The modelled velocities along the EGIG traverse are now larger by a factor between 1.4 and 1.9., and the relative deviations $\Delta A_r(h_s)$ are smaller than for scenario I-S; in fact $\Delta A_r(h_s)$ generally lies below 100% except at P 1, P 12 – P 15, with a maximum of 941% at P 14. The differences in the polar angles, $|\Delta\Theta|$, remain essentially the same.

We conclude that whereas the enhanced apparent fluidity of the Pleistocene ice has moved the modelled velocities along the EGIG-traverse towards the observed values, the adjustment is not sufficient.

3.5.3. Comparison of measured with computed EGIG-velocities using computations with freely evolving surface geometry. Besides the above fixed domain simulations with the prescribed topography inferred from the data, computations were also performed with a freely evolving upper surface that is subject to prescribed snowfall and surface melting. The idea was to adjust certain free model parameters such that the modelled ice surface topographies would agree as far as possible with the observed surface topography. Such a procedure seems to be more appro-

priate anyhow, because the original topographic data needed smoothing in order that the computed velocities would not oscillate unrealistically. The reason for this was not numerical instability but lack of precision in the measured surface heights. In what follows, we shall describe results from two computations with free ice thickness, but with today's climatic conditions at the free surface held constant; thus, contrary to the preceding computations, the ice-age-temperature variations are not accounted for.

In the first computation we employ the following conditions: $E = 3$ and basal sliding throughout (i.e. at both temperate and cold basal points) with the frictional heat accounted for. The free surface geometry now differs from that of the measurements, but the horizontal surface velocities along the EGIG-traverse can still be evaluated. Table 4 compares the measured EGIG-velocities (speeds and polar angles) with those of the model at the positions P 1 to P 17. In addition to the previous Table 3 it contains in column 4 the modelled basal speeds, $v_H^{\mathrm{mod}}(h_b)$. This allows a direct comparison of the contributions of sliding and gliding (due to creep deformation over the depth). Overall, the EGIG-velocities $v_H^{\mathrm{mod}}(h_s)$ agree better with the measured EGIG-speeds than in the computations of scenario I-S-E=3. However, the polar angles now deviate more from the measured values because the free surface is free to evolve.

At position P 1, $v_H^{\mathrm{mod}}(h_s)$ is now larger than $v_H^{\mathrm{meas}}(h_s)$, a fact that is expressed by the negative sign in the relative deviation $\Delta A_r(h_s) = -8.5\%$, which for scenario I-S-E=3 was as large as 138%. This increase of the EGIG velocities at P 1 is, however, only in parts due to the sliding that is incorporated in this computation. The sliding velocity $v_H^{\mathrm{mod}}(h_b)$ at P 1 with its $22.97\,\mathrm{m\,a^{-1}}$ is only about 20% of the modelled EGIG-velocities there. The increase of the computed EGIG-velocity at P 1 can be traced back in this case to the change of surface topography. At positions P 2 to P 7 the relative deviations $|\Delta A_r(h_s)|$ are of the order of 5%, in excellent agreement with the observations. Somewhat striking is the large value $\Delta A_r(h_s) = 234.5\%$ at position P 12. It is at this location, where the computed surface height assumes its maximum along the EGIG-traverse. In the scenarios I-S and I-S-E=3 this role was played by position P 14, and $\Delta A_r(h_s)$ reached a maximum in this location for these scenarios. Here it is, however, no longer appropriate to attribute the large deviations to accidental errors in the ice topography, because the latter is now determined by computations. It is evident that the model is not ideally capable of reproducing regions with small free surface slopes close to domes, obviously a demonstration of the nonuniformity of the validity of the shallow ice approximation. At P 14 – P 17, $\Delta A_r(h_s)$ is approximately -50%; the computed EGIG-velocities are too large in these positions.

At P 13 and P 14 the difference of the polar angle as obtained from observations and computations is larger than 180°, but, of course, its complement to 360° is then smaller than 180° and precisely indicates the error in the orientation of the velocity. It also comes as no surprise that the maximum errors of the

orientation arise where the surface speeds are smallest. Overall, the agreement of the orientations of the computed velocieties along the EGIG-profile with those of the observations is fair.

Table 4. Same as in Table 3, but now as obtained under conditions for which the free surface has been freely evolving for 50 000 years under steady driving conditions. Columns are the same as in Table 3, except that column 4 has been added which lists the modelled basal ice speed in m a^{-1}. At P 13 and P 14 both, the polar angle and its complement to 360° are listed. For details see also caption to Table 3.

Position	$v_H^{\text{meas}}(h_s)$ [m a^{-1}]	Θ^{meas} [°]	$v_H^{\text{mod}}(h_b)$ [m a^{-1}]	$v_H^{\text{mod}}(h_s)$ [m a^{-1}]	Θ^{mod} [°]	$\Delta A_r(h_s)$ [%]	$\Delta\Theta$ [°]
P 1	109.71	203.14	22.97	119.91	193.32	−8.5	9.82
P 2	88.28	206.34	15.07	86.44	200.96	2.1	5.38
P 3	70.71	209.91	11.49	67.21	204.63	5.2	5.28
P 4	59.07	213.35	9.54	56.02	207.23	5.4	6.12
P 5	47.75	202.40	7.96	45.81	207.83	4.2	−5.43
P 6	39.96	202.17	6.83	37.18	205.42	7.5	−3.25
P 7	31.40	200.60	5.58	29.92	206.35	5.0	−5.75
P 8	25.67	197.76	4.23	23.20	208.70	10.7	−10.94
P 9	18.76	194.73	3.01	16.27	210.96	15.3	−16.23
P 10	13.38	189.73	2.06	10.45	215.04	28.0	−25.31
P 11	9.88	182.79	1.26	6.05	221.02	63.3	−38.23
P 12	6.99	172.80	0.45	2.09	239.75	234.5	−66.95
P 13	4.21	144.46	0.71	3.39	346.43	24.2	−201.97
P 13							158.03*
P 14	3.54	95.56	1.52	7.31	358.30	−51.6	−262.74
P 14							97.26*
P 15	4.83	62.10	2.76	11.99	4.07	−59.7	58.03
P 16	7.58	44.47	4.44	18.06	8.28	−58.0	36.19
P 17	12.46	33.73	6.06	24.91	9.96	−50.0	23.77

In the next computation the model conditions are the same as above except that sliding is now restricted to the temperate basal regions; the comparison between the modelled and measured EGIG-velocities is given in Table 5. The relative deviations $|\Delta A_r(h_s)|$ of the measured from the modelled EGIG-velocities are now in all positions less than 100% with a maximum of 71.9% at P 17 and a minimum of 0.2% at P 2. Over most of the EGIG-traverse the computed surface velocities are larger than those observed, the reason being that at the positions where this happens (P 5 – P 14) the free surface heights are too large. Because of the restricted sliding in this, as opposed to the previous, computation, less ice is

transported to the margin. Notice also the values of the basal velocities $v_H^{\mathrm{mod}}(h_b)$ in Column 4 of Table 5 which differ from zero only at the positions P 1 to P 3. At these positions, the ice thicknesses of the two computations are very similar, implying that the deviations $|\Delta A_r(h_s)|$ are relatively small. This is exactly the other way around at positions P 16 and P 17. Here, $\Delta A_r(h_s)$ have opposite signs, a fact that is likely due to the small surface slopes.

Table 5. Same as in Table 4 but now for sliding arising only at temperate basal spots. In P 14 – P 17 both the polar angle and its complement to 360° are listed. For details, see also caption to Table 3.

Position	$v_H^{\mathrm{meas}}(h_s)$ [m a^{-1}]	Θ^{meas} [°]	$v_H^{\mathrm{mod}}(h_b)$ [m a^{-1}]	$v_H^{\mathrm{mod}}(h_s)$ [m a^{-1}]	Θ^{mod} [°]	$\Delta A_r(h_s)$ [%]	$\Delta\Theta$ [°]
P 1	109.71	203.14	26.48	135.45	191.82	−19.0	11.32
P 2	88.28	206.34	15.39	88.41	203.03	−0.2	3.31
P 3	70.71	209.91	2.90	63.81	211.24	10.8	−1.33
P 4	59.07	213.35	0.00	52.89	216.96	11.7	−3.61
P 5	47.75	202.40	0.00	50.00	209.73	−4.5	−7.33
P 6	39.96	202.17	0.00	44.39	203.64	−10.0	−1.47
P 7	31.40	200.60	0.00	38.30	206.02	−18.0	−5.42
P 8	25.67	197.76	0.00	30.12	210.13	−14.8	−12.37
P 9	18.76	194.73	0.00	21.88	213.51	−14.3	−18.78
P 10	13.38	189.73	0.00	15.68	217.12	−14.7	−27.39
P 11	9.88	182.79	0.00	11.64	224.58	−15.1	−41.79
P 12	6.99	172.80	0.00	8.07	233.51	−13.4	−60.71
P 13	4.21	144.46	0.00	5.39	256.08	−21.9	−111.62
P 14	3.54	95.56	0.00	4.71	279.11	−24.8	−183.55
P 14							176.45*
P 15	4.83	62.10	0.00	4.47	300.86	8.1	−238.76
P 15							121.24*
P 16	7.58	44.47	0.00	5.01	331.49	51.3	−287.02
P 16							72.98*
P 17	12.46	33.73	0.00	7.25	350.48	71.9	−316.75
P 17							43.25*

The orientations of the computed EGIG-velocities at P 1 to P 8 are fairly well reproduced; however, the differences $|\Delta\Theta|$ are now somewhat larger. At P 14, there arises an almost perfect inversion ($\Delta\Theta = 176.45°$). This result is not surprising since position P 14 is where the surface height along the EGIG-traverse reaches its maximum. The agreement of the orientation of the surface velocities at P 15 to P 17 is also worse than in the previous computation, probably because the North dome has moved towards the NE.

To compare the last two computations objectively, we have calculated the means

$$\overline{|\Delta A_r(h_s)|} = \frac{\sum_{i=1}^{17} |\Delta A_r(h_s)|_i}{17}, \qquad \overline{|\Delta\Theta|} = \frac{\sum_{i=1}^{17} |\Delta\Theta|_i}{17} \tag{3.10}$$

over all 17 positions and found the results of Table 6. Accordingly, the moduli of the surface velocities are better reproduced in the second computation, and their orientations are in better agreement in the first. Because we regard the speeds as more significant, the conditions of the second computation are probably closer to reality.

Table 6. Mean values of the moduli of the relative deviations $\Delta A_r(h_s)$ and the absolute deviations $\Delta\Theta$ for the seventeen selected points along the EGIG-traverse (see Eqs. (3.8) and (3.9)) for the steady-state computations with sliding overall (a) and that with sliding restricted to the temperate basal spots (b).

	$\overline{\lvert\Delta A_r(h_s)\rvert}$ [%]	$\overline{\lvert\Delta\Theta\rvert}$ [°]
a	37.2	33.6
b	19.1	42.4

4. Concluding remarks and outlook

For the Greenland Ice Sheet and probably all large ice sheets, the equilibrium temperature distribution is an unrealistic concept to estimate the temperature distribution for present climatic conditions. This statement holds true for all times through the last glacial cycle except perhaps the climatic minimum at 16 ka BP. The present temperature distribution in the Greenland Ice Sheet is affected by the last glacial cycle (Wisconsinan Ice Age), and to some extent the Illinoian Ice Age, as well as by the thermal inertia of the uppermost part of the rock bed. The temporal variation of the surface (air) temperature contributes significantly to the temporal and spatial distribution of the heat flow across the ice-rock interface, as it may vary from 33 to 43 mW m^{-2}.

By using various scenarios it was shown (but is not demonstrated here) that some parts of the basal area – probably rather small – were and are temperate, but that the locations where ice cores were drilled were probably never temperate. This statement holds even when the free surface is varied along with the climate driving, because the base can only become colder in this instance. Furthermore, the exact temporal variation of the homologous temperature at the base of "Dye 3", "Summit" and "Camp Century" depends on the mechanical and thermal properties of the ice, the thermal response of the rigid rock bed and the climate driving force through the surface temperature through time.

These inferences are drawn by using a restricted number of scenarios. The climate driving temperature was drastically simplified from the Vostok data. The

rock bed was assumed to be rigid and so the deformation of the lithosphere and the astenosphere were ignored, and the free-surface geometry was held fixed. These effects were thought to be of negligible influence, and in any case a description is possible only on the basis of unreliable data.

This review explained the theory upon which the thermomechanical processes of land-based ice sheets are based, and how this theory is reduced by a scaling analysis to the so-called shallow ice approximation. This turned out to be the lowest order outer solution of a matched asymptotic perturbation scheme valid except in a near margin boundary layer and in the vicinity of ice divides([3]). Numerical solution of the governing equations are nevertheless generally constructed through the entire ice sheet on the premise that the two inner regions are passive. While this seems to be correct for the near-margin layer, comparison of computed velocities along the EGIG-profile (and obtained with various computational scenarios) with the measured ones indicates that this is not so for the ice divide region. This conclusion is justified because deviations of the computed and measured velocities are systematically larger close to the divide than elsewhere.

Of course, authors of papers on ice divide analysis are aware of this fact [6, 28–31, 44, 73, 78, 133, 166, 173], but no attempt has so far been made to construct near-ice-divide solutions of the full Stokes equations. BLATTER [6] has made a first attempt towards that end, but the works of DAHL-JENSEN [28–31], REEH [160–163] and RITZ [164–167] and associates, intended to achieve this and known under the terms "longitudinal stress" or "longitudinal stretching effects" [15, 67, 151] cannot, in general, be systematically extended to embrace eventually the full Stokes equations. The scaling analysis of this article shows how it should be done, either by a formal perturbation or – and numerically more efficiently – by iteration; we are presently doing this.

Ice shield analyses need other, equally important amendments. The constitutive model of this article is that of a fluid and therefore necessarily isotropic. However, ice at depth is strongly anisotropic [27], while at formation from sintered snow in the surface layer it is isotropic. This stress-induced transition has only recently been incorporated into the first models [49, 131, 174, 175]. Their incorporation into ice sheet analyses and, in particular, the construction of reduced model equations by implementing the shallowness assumption is still ahead of us.

Acknowledgments

The work of K. HUTTER was partly supported by the A. v. Humboldt Foundation and the Max Planck Society through the Max Planck prize, that of

([3]) In the terminology of perturbation theory the outer region is that part of the domain of integration in which the perturbation solution of the unstretched equation is a valid approximation. The inner region is where the perturbation expansion of the stretched equation is valid. These latter regions are here the marginal zone and the neighbourhood of the ice divide [44].

R. CALOV by the Deutsche Forschungsgemeinschaft. We thank Prof. L.W. MORLAND for his review of an earlier version of this paper and for his help with the English wording. The file with the digitized topography of the Greenland Ice Sheet was given to us by Dr. ANNE LETRÉGUILLY. We also acknowledge the help received from D. BARAL and Y. WANG in the production of the extensive reference list.

References

1. J.M. BARNOLA, D. RAYNAUD, Y.S. KOROTKEVICH and C. LORIUS, *Vostok ice core provides 160 000-year record of atmospheric* CO_2, Nature, **329**, 408–414, 1987.
2. J.M. BARNOLA, P. PIMIENTA, D. RAYNAUD and Y.S. KOROTKEVICH, CO_2*-climate relationship as deduced from the Vostok ice core: a re-examination based on new measurements and on a re-evaluation of the air-dating*, Tellus, **43B**, 83–90, 1991.
3. M. BENDER, L.D. LABEYRIE, D. RAYNAUD and C. LORIUS, *Isotropic composition of atmospheric* O_2 *in ice linked with deglaciation and global primary productivity*, Nature, **318**, 349–352, 1985.
4. G.E. BIRCHFIELD, J. WEERTMAN and A. LUNDE, *A Paleoclimate model of Northern Hemisphere ice sheets*, Quat. Res., **15**, 126–142, 1981.
5. H. BLATTER, *Effect of climate on the cryosphere*, Züricher Geographische Schriften, Geographisches Institut, ETH Zürich, **41**, 1991.
6. H. BLATTER, *Velocity and stress fields in grounded glaciers: a simple algorithm for including deviatoric stress gradients*, J. Glaciol., **41**, 333–344, 1995.
7. H. BLATTER and K. HUTTER, *Polythermal conditions in arctic glaciers*, J. Glaciol., **37**, 126, 261–269, 1991.
8. G.S. BOULTON, G.D. SMITH and L.W. MORLAND, *The reconstruction of former ice sheets and their mass balance characteristics using a nonlinearly viscous flow model*, J. Glaciol., **30**, 105, 140–152, 1984.
9. W.J. BÖHMER and K. HERTERICH, *A simplified 3-D ice sheet model including ice shelves*, Ann. Glaciol., **14**, 17–19, 1990.
10. R.J. BRAITHWAITE and O.B. OLESEN, *Calculation of glacier ablation from air temperature, West Greenland*, [in:] Glacier Fluctuations and Climatic Change, J. OERLEMANS [Ed.], Kluwer, 219–233, 1989.
11. A.J. BROCCOLLI and S. MANABE, *The influence of continental ice, atmospheric* CO_2*, and land albedo on the climate of the last glacial maximum*, Climate Dyn., **1**, 87–99, 1987.
12. W.S. BROECKER, *Carbon dioxide circulation through ocean and atmosphere*, *Nature*, **308**, 602, 1984.
13. W.S. BROECKER, D.M. PETEET and D. RIND, *Does the ocean-atmosphere system have more than one stable mode of operation*, Nature, **315**, 21–26, 1985.
14. W. BROECKER and G.H. DENTON, *The role of ocean-atmosphere reorganizations in glacial cycles*, Geochimica et Cosmochimica Acta, **53**, 2465–2501, 1989.
15. W.F. BUDD, *Ice flow over bedrock perturbations*, J. Glaciol., **9**, 55, 29–48, 1970.
16. W.F. BUDD and D. JENSSEN, *Numerical modelling of glacier systems*, IAHS Publ., **104**, 257–291, 1975.
17. W.F. BUDD and D. JENSSEN, *The dynamics of the Antarctic ice sheet*, Ann. Glaciol., **12**, 16–22, 1989.
18. W.F. BUDD, D. JENSSEN and I.N. SMITH, *A threedimensional time-dependent model of the West Antarctic ice sheet*, Ann. Glaciol., **5**, 29–36, 1984.

19. W.F. BUDD and U. RADOK, *Glaciers and other large ice massers*, Rep. Prog. Phys., **34**, 1–70, 1971.

20. W.F. BUDD and I.N. SMITH, *Large-scale numerical modelling of the Antarctic ice sheet*, Ann. Glaciol., **3**, 42–49, 1982.

21. W.F. BUDD, T.H. JACKA, D. JENSSEN, U. RADOK and N. YOUNG, *Derived physical characteristics of the Greenland ice sheet*, Publication no. 23, University of Melbourne, Meteorology Department, 1982.

22. W.F. BUDD and N.W. YOUNG, *Application of modelling techniques to measured profiles of temperature and isotopes*, [in:] The Climatic Record in Polar Ice Sheets, G. DE Q. ROBIN [Ed.], Cambridge University Press, Cambridge, UK. 150–157, 1983.

23. W.F. BUDD and I.N. SMITH, *The state of balance of the Antarctic ice sheet, an updated assessment 1984*, [in:] Glaciers, Ice Sheets and Sea Level: Effects of a CO_2-Induced Climatic Change, DOE/ER/60235-1, National Academy Press, Washington, 172–177, 1985.

24. W.F. BUDD and T.H. JACKA, *A review of ice rheology for ice sheet modelling*, Cold Reg. Sci. Technol., **16**, 107–144, 1989.

25. R. CALOV, *Das thermomechanische Verhalten des Grönländischen Eisschildes unter der Wirkung verschiedener Klimaszenarien – Antworten eines theoretisch-numerischen Modells*, Dissertation, Institut für Mechanik, TH Darmstadt, 1994.

26. R. CALOV and K. HUTTER, *The thermomechanical response of the Greenland Ice Sheet to various climate scenarios*, Climate Dyn., **12**, 243–260, 1996.

27. O. CASTELNAU, TH. THORSTEINSSON, S. KIPFSTUHL, P. DUVAL and G.R. CANOVA, *Modelling fabric developement along the GRIP ice core, central Greenland*, Ann. Glaciol., **23**, 194–201, 1996.

28. D. DAHL-JENSEN, *Steady thermomechanical flow along two-dimensional flow lines in large grounded ice sheets*, J. Geophys. Res., **94**, (B8), 10 355–10 362, 1989.

29. D. DAHL-JENSEN, *Two-dimensional thermo-mechanical modelling of flow and depth-age profiles near the ice divide in central Greenland*, Ann. Glaciol., **12**, 31–36, 1989.

30. D. DAHL-JENSEN and S.J. JOHNSEN, *Paleotemperature still exist in Greenland ice sheet*, Nature, **320**, 250–252, 1986.

31. D. DAHL-JENSEN and N.S. GUNDESTRUP, *Constitutive properties of ice at Dye 3, Greenland*, [in:] The Physical Basis of Ice Sheet Modelling, IAHS, **170**, 31–43, 1987.

32. W. DANSGAARD, H.B. CLAUSEN, N. GUNDESTRUP, C.U. HAMMER, S.F. JOHNSEN, P.M. KRISTINSDOTTIR and N. REEH, *A New Greenland Deep Ice Core*, Science, **218**, 1273–1277, 1982.

33. P. DUVAL, *The role of the water content on the creep rate of polycristalline ice. In isotopes and impurities in snow and ice*, IAHS, **118**, 29–33, 1977.

34. P. DUVAL, *Mécanisme de la déformation plastique de la glace polycristalline*, La Houille Blanche, **6/7**, 499–503, 1984.

35. M.B. ESCH and K. HERTERICH, *A two-dimensional coupled atmosphere-ice sheet-continent model designed for paleoclimatic simulations*, Ann. Glaciol., **14**, 55–57, 1990.

36. A. FABRÉ, A. LETRÉGUILLY, C. RITZ and A. MANGENEY, *Greenland under changing climates: sensitivity experiments with a new three-dimensional ice sheet model*, Ann. Glaciol., **21**, 1–7, 1995.

37. A.C. FOWLER, *The use of a rational model in the mathematical analysis of polythermal glacier*, J. Glaciol., **24**, 443–456, 1979.

38. A.C. FOWLER, *A theoretical treatment of the sliding of glaciers in the absence of cavitation*, Phil. Trans. R. Soc. London, **298**, 1445, 637–685, 1981.

39. A.C. FOWLER, *A sliding law of glaciers of constant viscosity in the presence of subglacial cavitation*, Proc. R. Soc. London, **407**, 147–170, 1981.

40. A.C. FOWLER, *Waves on glaciers*, J. Fluid Mech., **120**, 283–321, 1982.

41. A.C. FOWLER, *A sliding law for temperate glaciers in the presence of subglacial cavitation*, Proc. R. Soc. London, 1984.

42. A.C. FOWLER, *Sub-temperate basal sliding*, J. Glaciol., **32**, 110, 3–5, 1986.

43. A.C. FOWLER, *Sliding with cavity formation*, J. Glaciol., **33**, 115, 255–267, 1987.

44. A.C. FOWLER, *Modelling ice sheet dynamics*, Geophys. Astrophys. Fluid Dynamics, **63**, 29–65, 1992.

45. A.C. FOWLER and D.A. LARSON, *On the flow of polythermal glaciers. I. Model and preliminary analysis*, Proc. R. Soc. London, **363**, 217–242, 1978.

46. A.C. FOWLER and D.A. LARSON, *The uniqueness of steady state flows of glaciers and ice sheets*, Geophys. J. Roy. Astr. Soc., **63**, 333–345, 1980.

47. M. FUNK, K. ECHELMEYER and A. IKEN, *Mechanisms of fast flow in Jacobshavns Isbrae, West Greenland. Part II. Modeling of englacial temperatures*, J. Glaciol., **40**, 136, 569–585, 1994.

48. J.W. GLEN, *The creep of polycrystalline ice*, Proc. R. Soc. London, **228**, 1175, 519–538, 1955.

49. N. AZUMA and K. GOTO-AZUMA, *An anisotropic flow law for ice-sheet ice and its implications*, Ann. Glaciol., **23**, 202–208, 1996.

50. R. GREVE, *Thermomechanisches Verhalten Polythermer Eisschilde – Theorie, Analytik, Numerik*, Berichte aus der Geowissenschaft, Shaker Verlag, Aachen, Germany, Dissertation, Institut für Mechanik, Technische Hochschule Darmstadt, Germany 1995.

51. R. GREVE, *Application of a polythermal three-dimensional ice sheet model to the Greenland Ice Sheet: Response to steady-state and transient climate scenarios*, J. of Climate, **10**, 901–918, 1997.

52. R. GREVE, *A continuum-mechanical formulation for shallow polythermal ice sheets*, Phil. Trans. R. Soc. London, **A 355**, 921–974, 1997.

53. R. GREVE and K. HUTTER, *Polythermal three-dimensional modelling of the Greenland ice sheet with varied geothermal heat flux*, Ann. Glaciol., **21**, 8–12, 1995.

54. R. GREVE and D.R. MACAYEAL, *Dynamic/thermodynamic simulations of Laurentide ice sheet instability*, Ann. Glaciol., **23**, 328–335, 1996.

55. I. HANSEN and R. GREVE, *Polythermal modelling of steady states of the Antarctic Ice Sheet in comparision with the real world*, Ann. Glaciol., **23**, 382–387, 1996.

56. I. HANSEN, R. GREVE and K. HUTTER, *Application of a polythermal ice sheet model to the Antarctic Ice Sheet: Steady-state solution and response to Milankovic cycles*, Proc. Fifth International Symposium on Thermal Engineering and Science for Cold Regions, Y. LEE and W. HALLET [Eds.], 89–96, 1996.

57. B.L. HANSEN and C.C. LANGWAY, Jr., *Deep core drilling in ice and ice core analysis at Camp Century, Greenland*, Antarctic J., **1**, 207–208, 1966.

58. K. HERTERICH, *On the flow within the transition zone between ice sheet and ice shelf*, [in:] Dynamics of the West Antarctic Ice Sheet, C.J. VAN DER VEEN and J. OERLEMANS [Eds.], D. Reidel (Dordrecht), 185–202, 1987.

59. K. HERTERICH, *A three-dimensional model of the Antarctic ice sheet*, Ann. Glaciol., **11**, 32–35, 1988.

60. K. HERTERICH, *Modellierung eiszeitlicher Klimaschwankungen*, Habilitationsschrift, Fachbereich Geowissenschaften, Universität Hamburg, 1990.

61. R.C.A. HINDMARSH and K. HUTTER, *Numerical fixed domain mapping solution of free-surface flows coupled with an evolving interior field*, Int. J. Numer. Anal. Methods Geomech., **12**, 437–459, 1988.

62. R.C.A. HINDMARSH, L.W. MORLAND, G.S. BOULTON and K. HUTTER, *The unsteady plane flow of ice-sheets, a parabolic problem with two moving boundaries*, Geophys. Astrophys. Fluid Dynamics, **39**, 3, 183–225, 1987.

63. R.C.A. HINDMARSH, G.S. BOULTON and K. HUTTER, *Modes of operation of thermomechanically coupled ice sheets*, Ann. Glaciol., **12**, 57–69, 1989.

64. W. HOFMANN, *Die Internationale Glaziologische Grönland-Expedition* EGIG, Z. Gletscherkd. Glazialgeol., **5**, 217–224, 1974.

65. R. LEB. HOOKE, *Flow law for polycrystalline ice in glaciers: comparison of theoretical predictions, laboratory data, and field measurements*, Rev. Geophys. Space Phys., **19**, 4, 664–672, 1981.

66. K. HUTTER, *Time-dependent surface elevation of an ice slope*, J. Glaciol., **25**, 247–266, 1980.

67. K. HUTTER, *The effect of longitudinal strain on the shear stress of an ice sheet. In defence of using stretched coordinates*, J. Glaciol., **27**, 95, 39–56, 1981.

68. K. HUTTER, *A mathematical model of polythermal glaciers and ice sheets*, Geophys. Astrophys. Fluid Dynamics, **21**, 201–224, 1982.

69. K. HUTTER, *Dynamics of glaciers and large ice masses*, Ann. Rev. Fluid Mech., **14**, 87–130, 1982.

70. K. HUTTER, *Glacier flow*, Am. Sci., **70**, 1, 26–34, 1982.

71. K. HUTTER, *Theoretical glaciology; material science of ice and the mechanics of glaciers and ice sheets*, D. Reidel Publishing Company, Dordrecht, Holland 1983.

72. K. HUTTER, *Mathematical foundation of flow of glaciers and large ice masses*, [in:] Mathematical Models and Methods in Mechanics, Banach Center Publ., **15**, PWN-Polish Scientific Publishers, Warsaw. 277–322, 1985.

73. K. HUTTER, *Thermo-mechanically coupled ice sheet response. Cold, polythermal, temperate*, J. Glaciol., **39**, 131, 65–86, 1993.

74. K. HUTTER and H. ENGELHARDT, *How useful is continum thermodynamics to formulate concepts of ice sheet dynamics?* Eidg. Tech. Hochschule, Zürich. Versuchsanst. Wasserbau, Hydrol. Glaziol. Mitt., 94, 163–210, 1988.

75. K. HUTTER and H. ENGELHARDT, *The use of continuum thermodynamics in the formulation of ice sheet dynamics*, Ann. Glaciol., **11**, 46–51, 1988.

76. K. HUTTER, H. BLATTER and M. FUNK, *A model computation of moisture content in polythermal glaciers*, J. Geophys. Res., **93**, (B10), 12205–12214, 1988.

77. K. HUTTER and L. VULLIET, *Gravity driven slow creeping flow of a thermoviscous body at elevated temperatures*, J. Thermal Stresses, **8**, 99–138, 1985.

78. K. HUTTER, S. YAKOWITZ and F. SZIDAROVSZKY, *A numerical study of plane ice sheet flow*, J. Glaciol., **32**, 111, 139–164, 1986.

79. K. HUTTER, S. YAKOWITZ and F. SZIDAROVSKY, *Coupled thermomechanical response of an axi-symmetric cold ice sheet*, J. Water Resources Research, **23**, 1327–1339, 1987.

80. P. HUYBRECHTS, *A three-dimensional time-dependent numerical model for polar ice sheets: some basic testing with a stable and efficient finite difference scheme*, Geografisches Institute VUB Report 86-1, p. 39, 1986.

81. P. HUYBRECHTS, *Dynamics of the Antarctic ice cap. Part II. Sensitivity experiments with a numerical ice sheet model with full thermo-mechanical coupling*, Proc. of the Belgian National Colloquium on Antarctic Research, 226–239, 1987.

82. P. HUYBRECHTS, *A 3-D model for the Antarctic ice sheet: a sensitivity study on the glacial-interglacial contrast*, Climate Dyn., **5**, 79–92, 1990.

83. P. HUYBRECHTS, *The Antarctic ice sheet during the last glacial-interglacial cycle: A three-dimensional experiment*, Ann. Glaciol., **14**, 115–119, 1990.

84. P. HUYBRECHTS, *The Antarctic ice sheet and environmental change: a three-dimensional modelling study*, Berichte zur Polarforschung, **99**, Alfred-Wegener-Institut, Bremerhaven 1992.

85. P. HUYBRECHTS, *Glaciological modelling of the Late Cenozoic East Antarctic ice sheet: stability or dynamism?* Geografiska Annaler, **75 A**, 4, 221–238, 1993.

86. P. HUYBRECHTS, *The present evolution of the Greenland ice sheet: an assessment by modelling*, Global and Planetary Change, **9**, 39–51, 1994.

87. P. HUYBRECHTS, A. LETRÉGUILLY and N. REEH, *The Greenland ice sheet and greenhouse warming*, Palaeogeography, Palaeoclimatology, Palaeoecology, Global and Planetary Change Section, **89**, 399–412, 1991.

88. P. HUYBRECHTS and J. OERLEMANS, *Evolution of the East Antarctic ice sheet: A numerical study of thermo-mechanical response patterns with changing climate*, Ann. Glaciol., **11**, 52–59, 1988.

89. P. HUYBRECHTS and J. OERLEMANS, *Response of the Antarctic ice sheet to future greenhouse warming*, Climate Dyn., **5**, 93–102, 1990.

90. D. JENSSEN, *A three-dimensional polar ice-sheet model*, J. Glaciol., **18**, 80, 373–389, 1977.

91. D. JENSSEN and J.A. CAMPBELL, *Heat conduction studies*, [in:] The Climatic Record In Polar Ice sheets, G. DE Q. ROBIN [Ed.], . Cambridge University Press, Cambridge, UK., 150–157, 1983.

92. S.J. JOHNSEN, H.B. CLAUSEN, W. DANSGAARD, K. FUHRER, N. GUNDESTRUP, C.U. HAMMER, P. IVERSEN, J. JOUNZEL, B. STAUFFER and J.P. STEFFENSEN, *Irregular glacial interstadials recorded in a new Greenland ice core*, Nature, **359**, 311–313, 1992.

93. J. JOUZEL, L. MERLIVAT and C. LORIUS, *Deuterium excess in an East Antarctic ice core suggests higher relative humidity at the oceanic surface during the last glacial maximum*, Nature, **299**, 688–691, 1982.

94. J. JOUZEL and L. MERLIVAT, *Deuterium and Oxygen 18 in Precipitation: Modelling of the isotopic effects during snow formation*, J. Geophys. Res., **89**, D7, 11749–11757, 1984.

95. J. JOUZEL, L. MERLIVAT, J.R. PETIT and C. LORIUS, *Climatic information over the last century deduced from a detailed isotopic record in the South Pole snow*, J. Geophys. Res., **88**, C4, 2693–2703, 1983.

96. J. JOUZEL, C. LORIUS, J.R. PETIT, C. GENTHON, N.I. BARKOV, V.M. KOTLYAKOV and V.M. PETROV, *Vostok ice core: a continuous isotope temperature record over the last climatic cycle (160,000 years)*, Nature, **329**, 403–408, 1987.

97. J. JOUZEL, G.L. RUSSEL, R.J. SUOZZO, R.D. KOSTER, J.W.C. WHITE and W.S. BROECKER, *Simulation of the HDO and $H_2^{18}O$ atmospheric cycles using the NASA GISS general circulation model: The seasonal cycle for present-day conditions*, J. Geophys. Res., **92**, D 12, 14739–14760, 1987.

98. J. JOUZEL, G. RAISBECK, J.P. BENOIST, F. YIOU, C. LORIUS, D. RAYNAUD, J.R. PETIT, N.I. BARKOV, Y.S. KOROTKEVICH and V.M. KOTLYAKOV, *A comparison of deep Antarctic ice cores and their implications for climate between 65,000 and 15,000 years ago*, Quat. Res., **31**, 135–150, 1989.

99. M. KUHLE, K. HERTERICH and R. CALOV, *On the ice age glaciation of the Tibetan Highlands and its transformation into a 3-D model*, GeoJournal, **19**, 2, 201–206, 1989.

100. L.D. LABEYRIE, J.S. DUPLESSY and P.L. BLANC, *Variations in mode of formation and temperature of oceanic deep waters over the past 125,000 years*, Nature, **327**, 477–482, 1987.

101. K. LAMBECK and M. NAKADA, *Constraints on the age and duration of the last interglacial period and on sea-level variations*, Nature, **357**, 125–128, 1992.

102. R. LeB. HOOK, C. RAYMOND, R.L. HOTCHKISS and R.J. GUSTAFSON, *Calculation of velocity and temperature in a polar glacier using the finite-element method*, J. Glaciol., **24**, 90, 131–146, 1979.

103. A. LETRÉGUILLY, P. HUYBRECHTS and N. REEH, *Steady-state characteristics of the Greenland ice sheet under different climates*, J. Glaciol., **37**, 125, 149–157, 1991.

104. A. LETRÉGUILLY, N. REEH and P. HUYBRECHTS, *Topographical data for Greenland*, Report, Alfred-Wegener-Institut für Polar- und Meeresforschung, Bremerhaven 1990.

105. A. LETRÉGUILLY, N. REEH and P. HUYBRECHTS, *The Greenland ice sheet through the last glacial-interglacial cycle*, Palaeogeography, Palaeoclimatology, Palaeoecology, Global and Planetary Change Section, **90**, 4, 385–394, 1991.

106. R.C. LILE, *The effect of anisotropy on the creep of polycrystalline ice*, J. Glaciol., **21**, 85, 475–483, 1978.

107. L. LLIBOUTRY, *Traité de glaciologie. Tome I and II*, Masson, Paris 1964-1965.

108. L. LLIBOUTRY, *General theory of subglacial cavitation and sliding of temperate glaciers*, J. Glaciol., **7**, 49, 21–58, 1968.

109. L. LLIBOUTRY, *The dynamics of temperate glaciers from the detailed viewpoint*, J. Glaciol., **8**, 53, 185–205, 1969.

110. L. LLIBOUTRY, *Loi de glissement d'un glacier sans cavitation*, Ann. Géophys., **31**, 2, 207–226, 1975.

111. L. LLIBOUTRY, *Physical processes in temperate glaciers*, J. Glaciol., **16**, 74, 151–158, 1976.

112. L. LLIBOUTRY, *Local friction laws for glaciers. A critical review and new openings*, J. Glaciol., **23**, 89, 67–95, 1979.

113. L. LLIBOUTRY, *A critical review of analytical approximate solutions for steady state velocities and temperatures in cold ice-sheets*, Z. Gletscherkd. Glazialgeol., **15**, 2, 135–148, 1981.

114. L. LLIBOUTRY, *Tectonphysique et géodynamique. Une synthése. Géologie structurale. Géophysique interne*, Masson Ed., 1982.

115. L. LLIBOUTRY, *Very slow flow of solids: Basics of modelling in geodynamics and glaciology*, Martinus Nijhoff, Dordrecht, Netherlands 1987.

116. L. LLIBOUTRY, *Realistic, yet simple bottom boundary conditions for glaciers and ice sheets*, J. Geophys. Res., **92**, b 9, 9101–9109, 1987.

117. L. LLIBOUTRY and P. DUVAL, *Various isotropic and anisotropic ices found in glaciers and polar ice caps and their corresponding rheologies*, Annales Geophysicae, **3**, 2, 207–224, 1985.

118. C. LORIUS and L. MERLIVAT, *Distribution of mean surface stable isotope values in East Antarctica: observed changes with depth in the coastal area*, IAHS 118, Proc. of the Grenoble Symposium, 127–137, 1977.

119. C. LORIUS, L. MERLIVAT, J. JOUZEL and M. POURCHET, *A 30,000-yr isotope climatic record from Antarctic ice*, Nature, **280**, 644–648, 1979.

120. C. LORIUS, J. JOUZEL, C. RITZ, L. MERLIVAT, N.I. BARKOV, Y.S. KOROTKEVITCH and V. KOTLYAKOV, *A 150,000 year climatic record from Antarctic ice*, Nature, **316**, 591–596, 1985.

121. D.R. MACAYEAL, *Ice-shelf backpressure: form drag versus dynamic drag*, [in:] Dynamics of the West Antarctic Ice Sheet, C.J. VAN DER VEEN and J. OERLEMANS [Ed.], Reidel., 141–16, 1987.

122. D.R. MACAYEAL, *Large-scale ice flow over a viscous basal sediment: Theory and application to ice stream B, Antarctica*, J. Geophys. Res., **94**, B 4, 4071–4087, 1989.

123. D.R. MACAYEAL and R.H. THOMAS, *Numerical modelling of ice-shelf motion*, Ann. Glaciol., **3**, 189–194, 1982.

124. D.R. MACAYEAL and R.H. THOMAS, *The effects of basal melting on the present flow of the Ross Ice Shelf, Antarctica*, J. Glaciol., **32**, 110, 72–86, 1986.

125. M.W. MAHAFFY, *A three-dimensional numerical model of ice sheets: Test on the Barnes ice cap, Northwest Territories*, J. Geophys. Res., **81**, 6, 1059–1066, 1976.

126. A. MANGENEY, *Modélisation de l'écoulement de la glace dans les callottes palaires: prise en compte d'une loi comportement anisotrope*, Thèse de Doctorat de l'Université Pierre et Marie Curie – Paris VI, 1996.

127. A. MANGENEY and F. CALIFANO, *The shallow-ice approximation for anisotropic ice – formulation and limits*, J. Geophys. Res., 1997 [in press].

128. A. MANGENEY, F. CALIFANO and K. HUTTER, *A numerical study of anisotropic ice, low-Reynolds numbers, free surface flows for ice sheet modelling*, J. Geophys. Res., 1997 [in press].

129. B.J. MCINNES and W.F. BUDD, *A cross-sectional model for West Antarctica*, Ann. Glaciol., **5**, 95–99, 1984.

130. J. MEYSSONNIER and A. PHILIP, *A model for tangent viscous behaviour of anisotropic ice*, Ann. Glaciol., **23**, 253–261, 1996.

131. L.W. MORLAND, *Glacier sliding down an inclined wavy bed*, J. Glaciol., **17**, 77, 447–462, 1976.

132. L.W. MORLAND, *Glacier sliding down an inclined wavy bed with friction*, J. Glaciol., **17**, 77, 463–477, 1976.

133. L.W. MORLAND, *Thermo-mechanical balances of ice sheet flows*, Geophys. Astrophys. Fluid Dynamics, **29**, 237–266, 1984.

134. L.W. MORLAND and I.R. JOHNSON, *Steady motion of ice sheets*, J. Glaciol., **25**, 229–246, 1980.

135. L.W. MORLAND and I.R. JOHNSON, *Effect of bed inclination and topography on steady isothermal ice sheets*, J. Glaciol., **28**, 71–90, 1982.

136. L.W. MORLAND and G.D. SMITH, *Influence of non-uniform temperature distribution on the steady motion of ice sheets*, J. Fluid Mech., **140**, 113–930, 1984.

137. L.W. MORLAND, G.D. SMITH and G.S. BOULTON, *Basal sliding relations deduced from ice sheet data*, J. Glaciol., **30**, 105, 131–139, 1984.

138. J.F. NYE, *The flow of glaciers and ice-sheets as a problem in plasticity*, Proc. R. Soc. London, **207**, 554–572, 1951.

139. J.F. NYE, *The mechanics of glacier flow*, J. Glaciol., **2**, 82–93, 1952.

140. J.F. NYE, *A comparison between the theoretical and the measured long profile of the Unteraar Glacier*, J. Glaciol., **2**, 103–107, 1952.

141. J.F. NYE, *The flow law of ice from measurements in glacier tunnels, laboratory experiments and the Jungfraufirn borehole experiment*, Proc. R. Soc. London, **219**, 477–489, 1953.

142. J.F. NYE, *The distribution of stress and velocity in glaciers and ice-sheets*, Proc. R. Soc. London, **239**, 113–133, 1957.

143. J.F. NYE, *A theory of wave formation on glaciers*, IASH, **47**, 139–154, 1958.

144. J.F. NYE, *The deformation of a glacier below an ice fall*, J. Glaciol., **3**, 387–408, 1959.
145. J.F. NYE, *The response of glaciers and ice-sheets to seasonal and climatic changes*, Proc. R. Soc. London, **256**, 559–584, 1960.
146. J.F. NYE, *The influence of climatic variations on glaciers*, IASH, **54**, 297–404, 1961.
147. J.F. NYE, *On the theory of the advance and retreat of glaciers*, Geophys. J.R. Astron. Soc., **7**, 431–456, 1963.
148. J.F. NYE, *The response of a glacier to changes in the rate of nourishment and wastage*, Proc. R. Soc. London, **275**, 87–112, 1963.
149. J.F. NYE, *The flow of a glacier in a channel of rectangular, elliptic or parabolic cross-section*, J. Glaciol., **5**, 661–690, 1965.
150. J.F. NYE, *Plasticity solution for a glacier snout*, J. Glaciol., **6**, 695–715, 1967.
151. J.F. NYE, *The effect of longitudinal stress on the shear stress at the base of an ice sheet*, J. Glaciol., **8**, 53, 207–213, 1969.
152. J.F. NYE, *A calculation on the sliding of ice over a wavy surface using a Newtonian viscous approximation*, Proc. R. Soc. London, **311**, 445–467, 1969.
153. J.F. NYE, *Glacier sliding without cavitation in a linear viscous approximation*, Proc. R. Soc. London, **315**, 1522, 381–403, 1970.
154. A. OHMURA, *New temperature distribution maps for Greenland*, Z. Gletscherkd. Glazialgeol., **23**, 1–45, 1987.
155. A. OHMURA and N. REEH, *New precipitation and accumulation maps for Greenland*, J. Glaciol., **37**, 140–148, 1991.
156. W.S.B. PATERSON, *Why ice-age ice is sometimes "soft"*, Cold Reg. Sci. Technol., **20**, 75–98, 1991.
157. J.R. PETIT, L. MOUNIER, J. JOUZEL, V.I. KOTLYAKOV and C. LORIUS, *Paleoclimatological and chronological implications of the Vostok core dust record*, Nature, **343**, 56–58, 1990.
158. U. RADOK, T.J. BROWN, D. JENSSEN, I.N. SMITH and W.F. BUDD, *On the surging potential of polar ice streams*. Part IV. *Antarctic ice accumulation basins and their main discharge regions*, Boulder CO, University of Colorado, Cooperative Institute for Research in Environmental Sciences/Parkville, Victoria, University of Melbourne, Meteorology Department, 1986.
159. C.F. RAYMOND, *Deformation in the vicinity of ice divides*, J. Glaciol., **29**, 103, 357–373, 1983.
160. N. REEH, *A flow-line model for calculating the surface profile and the velocity, strain rate and stress fields in an ice sheet*, J. Glaciol., **34**, 116, 46–54, 1988.
161. N. REEH, *The age-depth profile in the upper part of a steady-state ice sheet*, J. Glaciol., **35**, 121, 406–417, 1989.
162. N. REEH, *Parameterization of melt rate and surface temperature on the Greenland ice sheet*, Polarforschung, **59**, 3, 113–128, 1991.
163. N. REEH, S.J. JOHNSEN and D. DAHL-JENSEN, *Dating the Dye 3 deep ice core by flow model calculations*, [in:] Greenland Ice Core: Geophysics, Geochemistry, and the Environment, Geophysical Monograph 33, C.C. LANGWAY, H. OESCHGER and W. DANSGAARD [Eds.], A. G. U., 57–65, 1985.
164. C. RITZ, *Exploitation du profil de températures mesuré dans la calotte glaciaire au Dôme C (Antarctide Orientale)*, Thése de Troisiéme Cycle de l'Université Scientifique et Médicale de Grenoble, 1980.
165. C. RITZ, *Time-dependent boundary conditions for calculation of temperature fields in ice sheets*, [in:] The Physical Basis of Ice Sheet Modelling, E.D. WADDINGTON and J.S. WALDER, IAHS Publication No. 170. 1987.

166. C. RITZ, *Interpretation of the temperature profile measured at Vostok, East Antarctica*, Ann. Glaciol., **12**, 138–144, 1989.
167. C. RITZ, L. LLIBOUTRY and C. RADO, *Analysis of a 870 m deep temperature profile at Dome C*, Ann. Glaciol., **3**, 284–289, 1982.
168. D.S. RUSSEL-HEAD and W.F. BUDD, *Ice-sheet flow properties derived from bore-hole shear measurements combined with ice-core studies*, J. Glaciol., **24**, 90, 117–130, 1979.
169. T.J.O. SANDERSON, *Equilibrium profile of ice shelves*, J. Glaciol., **22**, 88, 435–460, 1979.
170. N.J. SHACKLETON, *Oxygen isotopes, ice volume and sea level*, Quat. Sci. Rev., **6**, 183–190, 1987.
171. N.J. SHACKLETON, M.A. HALL and SHUXI CANG, *Carbon isotope data in core V19-30 confirm reduced carbon diobon dioxide concentration in the ice age atmosphere*, Nature, **306**, 319–322, 1983.
172. B. STAUFFER, *Dating of ice by radioactive isotope*, [in:] Dahlem Conference, The environmental Record in Glaciers and Ice Sheets, H. OESCHGER and C.C. LANGWAY Jr. [Eds.], 123–139, 1989.
173. F. SZIDAROVSZKY, K. HUTTER and S. YOKOWITZ, *Computational ice-divide analysis of a cold plane ice sheet under steady conditions*, Ann. Glaciol., **12**, 170–177, 1989.
174. B. SVENDSEN and K. HUTTER, *On the continuum modelling of induced anisotropy in polycrystals*, Quarterly of Applied Mathematics, 1995.
175. B. SVENDSEN and K. HUTTER, *A continuum approach for modelling-induced anisotropy in glaciers and ice sheets*, Ann. Glaciol., **23**, 262–269, 1995.
176. D.L. TURCOTTE and G. SCHUBERT, *Geodynamics*, John Wiley, New York, p. 440, 1982.
177. E.D. WADDINGTON, *Geothermal heat flux beneath ice sheets*, [in:] The Physical Basis of Ice Sheet Modeling, IAHS, **170**, 217–226, 1987.
178. J. WEERTMANN, *On the sliding of glaciers*, J. Glaciol., **3**, 21, 33–38, 1957.
179. J. WEERTMAN, *Deformation of floating ice shelves*, J. Glaciol., **3**, 38–42, 1957.
180. J. WEERTMAN, *Stability of ice-age ice sheets*, J. Geophys. Res., **66**, 11, 3783–3792, 1961.
181. J. WEERTMANN, *Mechanism for the formation of inner moraines found near the edge of cold ice caps and ice sheets*, J. Glaciol., **3**, 30, 965–978, 1961.
182. J. WEERTMANN, *The theory of glacier sliding*, J. Glaciol., **5**, 39, 287–303, 1964.
183. J. WEERTMANN, *An examination of the Lliboutry theory of glacier sliding*, J. Glaciol., **6**, 46, 489–494, 1967.
184. J. WEERTMAN, *Comparison between measured and theoritical temperature profiles of the Camp century, Greenland borehole*, J. Geophys. Res., **73**, 2691–2700, 1968.
185. J. WEERTMANN, *In defense of a simple model of glacier sliding*, J. Geophys. Res., **76**, 26, 6485–6487, 1971.
186. J. WEERTMANN, *General theory of water flow at the base of a glacier or ice sheet*, Rev. Geophys. Space Phys., **10**, 1, 187–333, 1972.
187. J. WEERTMANN, *The unsolved general glacier sliding problem*, J. Glaciol., **23**, 89, 97–115, 1979.
188. M. WEIS, K. HUTTER and R. CALOV, 250 000 *years in history of Greenland's ice sheet*, Ann. Glaciol., **23**, 359–363, 1996.

DEPARTMENT OF MECHANICS
TU DARMSTADT, DARMSTADT, GERMANY.
e-mail:hutter@mechanik.tu-darmstadt.de

Received February 21, 1997; new version May 28, 1997.